

ORIGINAL ARTICLE

A multi-analytical approach applied to pottery from Oman as a key to understanding ancient Indian Ocean maritime trade

Daniele Zampierin¹  | Patrícia Moita² | Silvia Lischi^{3,4} |
Marieke van Aerde⁵  | Pedro Barrulas²  | José Mirão²

¹Berlin Graduate School of Ancient Studies, Freie Universität Berlin, Berlin, Germany

²HERCULES Laboratory, University of Évora, Évora, Portugal

³Dipartimento di Civiltà e forme del sapere, University of Pisa, Pisa, Italy

⁴Faculty of Asian and Middle Eastern Studies, University of Oxford, Oxford, United Kingdom of Great Britain and Northern Ireland

⁵Faculty of Archaeology, Leiden University, Leiden, Netherlands

Correspondence

Daniele Zampierin, Berlin Graduate School of Ancient Studies, Freie Universität Berlin, Hittorfstraße 18, 14195, Berlin, Germany.
Email: daniele.zampierin@hotmail.com

Funding information

Erasmus Mundus Joint Master in Archaeological Material Science

Abstract

The populations in Sumhuran (third/second century BCE to fifth century CE) and Hamr al-Sharqiya 1 (HAS1) (first millennium BCE to first/second century CE) were involved in one of the most important examples of large-scale trade systems in antiquity: the maritime network connecting the coasts of the Indian Ocean. This research focuses on a total of 35 southwestern Arabian and Indian pottery sherds from both the settlements of Sumhuran and Hamr al-Sharqiya 1, analysed through a multi-analytical complementary approach. This study intends to test the input potential of this type of approach applied to ceramics in the context of the Indian Ocean trade network. The techniques adopted are powder X-ray diffraction, optical microscopy, inductively coupled plasma–mass spectrometry and scanning electron microscopy coupled with energy-dispersive X-ray spectroscopy. The results obtained allow the identification of eight distinct groups, each characterized by unique (textural, mineralogical, geochemical) signatures, providing specific clues for determining their provenance, specifically from the Indian subcontinent and southwestern Arabia. This paper shows the importance of this type of archaeometric study that must be integrated into a transdisciplinary approach.

KEYWORDS

archaeometry, ceramics, Dhofar, Indian Ocean trade, Khor Rori

This is an open access article under the terms of the [Creative Commons Attribution-NonCommercial](https://creativecommons.org/licenses/by-nc/4.0/) License, which permits use, distribution and reproduction in any medium, provided the original work is properly cited and is not used for commercial purposes.

© 2024 The Authors. *Archaeometry* published by John Wiley & Sons Ltd on behalf of University of Oxford.

ARCHAEOLOGICAL AND HISTORICAL BACKGROUND

Between the end of the third and the beginning of the second century BCE, the south Arabian kingdom of Hadramawt established an outpost called Sumhuram in Dhofar, the southern region of the Sultanate of Oman, with the probable aim of facilitating the collection of the locally produced frankincense (Buffa, 2019). At that time, the Dhofar region was already inhabited, as highlighted by archaeological traces found during the Trans Arabian Expedition (Zarins, 2001) and by the excavations conducted at Hamr al-Sharqiya 1 (HAS1),ⁱ a settlement located on the coastal plateau of Inqitat, just a few kilometres away from Sumhuram (Lischi, 2019, 2023). Sumhuram and HAS1 are nowadays included within the same archaeological area known as Khor Rori (Figure 1).

The earliest occupation layers in Sumhuram reveal the contemporary presence of typologically identified southwestern Arabianⁱⁱ and Indianⁱⁱⁱ ceramics (Buffa, 2019). The coexistence of the two ceramic groups ended around the third century CE, while the settlement continued to be inhabited until the beginning of the fifth century CE (Buffa, 2019, pp. 266–267). The central location of Sumhuram, dominating the estuary of Wadi Darbat and the surrounding area, was highly strategic along the coast of the southern part of the Arabian Peninsula and along the Indian Ocean maritime trade route. In fact, the presence of warehouses and the considerable number of imported materials found within the city emphasize the commercial nature of the settlement (Avanzini & Pavan, 2011; Lischi, 2021). The archaeological site was first excavated in the 1950s by the American Foundation for the Study of Man^{iv} (Albright, 1982) and then by the Italian Mission to Oman^v from 1999 until 2019 (Buffa, 2019).

The area of HAS1 was already in use around the first half of the first millennium BCE and abandoned by the end of the first or beginning of the second century CE (Lischi, 2018, 2023). The excavation of HAS1 started in 2016 under IMTO and successively continued under the DHOMIAP^{vi} research project. The settlement, roughly 2 ha in size, was composed of several circular or sub-circular structures, and its material assemblage included a large number of artefacts identified as imports (Lischi, 2019, 2023; Lischi, Pavan, & Fusaro, 2020).

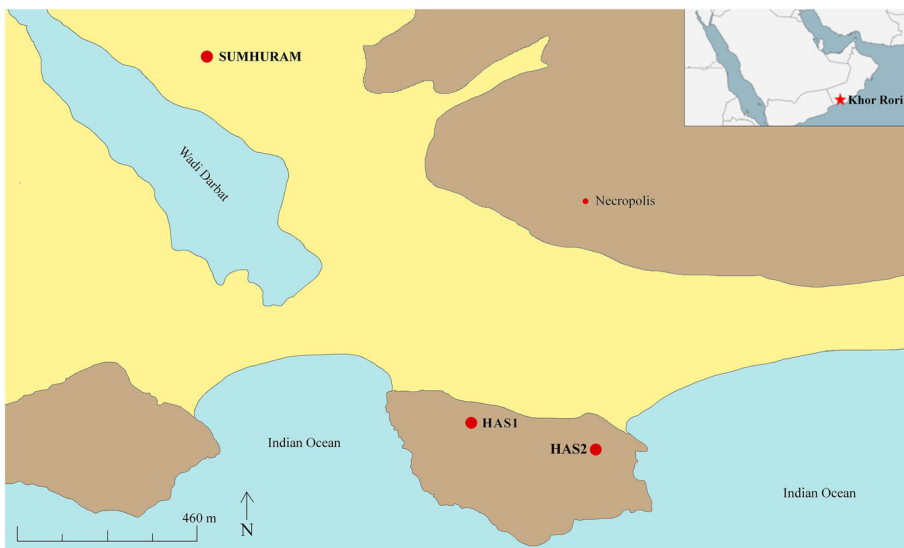


FIGURE 1 Schematic map of the archaeological site of Khor Rori, highlighting the locations of Sumhuram, HAS1, HAS2 and the necropolis. In the top right corner is a mute map of the location of Khor Rori within the Arabian Peninsula.

The coeval occupation of Sumhuram and HAS1 and the co-occurrence, in both settlements, of southwestern Arabic, Dhofari and imported materials from regions around the Indian Ocean represent a unique context to explore the movement of goods across the western Indian Ocean. In particular, the context of Sumhuram and HAS1 provides the opportunity to investigate what types of materials were reaching the Dhofar region and where they were arriving from.

MATERIALS AND METHODS

This paper presents an archaeometric study on southwestern Arabian and Indian ceramics found in Khor Rori (Lischi, 2022). The analysed materials include (Table 1) 18 sherds from HAS1 and 17 from Sumhuram, representing a variety of Indian and southwestern Arabian fabric recorded within the two sites (Lischi, 2019, 2022; Lischi, Pavan, & Fusaro, 2020; Pavan, 2017). This study aims to explore how methodologies already applied in other regions and chronologies (Beltrame et al., 2019; Borowski et al., 2015; Finlay et al., 2012; Maritan et al., 2009; Miriello et al., 2015; Seetha & Velraj, 2016; Tsoupra et al., 2022) contribute to understanding the movement of goods within the context of the Indian Ocean trade network. By integrating archaeometric results with sherd provenance based on typological classification by Pavan (2017) and Lischi et al. (2022), this study aims to enhance the understanding of the materials' origins and characteristics. The multi-analytical approach adopted,^{vii} which includes thin-section petrography (optical microscopy, OM), powder X-ray diffraction (PXRD), scanning electron microscopy with energy-dispersive X-ray spectroscopy (SEM-EDS) and inductively coupled plasma-mass spectrometry (ICP-MS), has already been proven extremely effective in obtaining the ceramic composition, technological characterization and provenance in previous studies in different research contexts (Beltrame et al., 2019; Borowski et al., 2015; Finlay et al., 2012; Maritan et al., 2009; Miriello et al., 2015; Seetha & Velraj, 2016; Tsoupra et al., 2022). For a comprehensive review of analytical methods commonly used in archaeometry, this research refers to Maritan (2019).

The data retrieved from chemical, mineralogical and textural analyses highlight specific details and clarify the classification of some of the ceramic fabrics previously defined by Pavan (2017) and Lischi et al. (2022), contributing to the development of a more comprehensive image of Khor Rori's ceramic corpora. Due to the invasive and partially destructive nature of the analyses conducted, all samples were first recorded through photography and some through 3D photogrammetry (Karasik & Smilansky, 2008; Mirulla, 2011).

Sample preparation

To perform mineralogical and chemical analyses, a fragment of the samples (roughly 10 g) was cut off using a circular Struers Discoplan saw to be less invasive. The pieces removed were then rinsed carefully with distilled water and ethanol before being dried at 40°C for 24 h. The subsequent powdering of the fragments was initialized by hand using an agate mortar and completed using the automatic mill Retsch PM100. The powders were then stored at 40°C to avoid moisture from getting into the samples. Loss on ignition (LOI) was determined by the calcination of dried samples in a muffle furnace (0.5 g) for 2 h at 1050°C. Simultaneously, a smaller piece was cut off to prepare the thin sections. To produce 30 µm-thick thin sections, the 'TS method' developed by Struers was adapted by adding EpoDye colourant to the impregnation mix.^{viii} This addition makes it possible to measure the porosity with image processing in future studies.

TABLE 1 List of the samples analysed in this paper and of relative information available (Buffa, 2019; Lischi, 2022; Pavan, 2017) before the archaeometric approach.




Samples from Sumhuram		Vessel shape	Vessel type	Macroscopic characteristics of the fabric	Provenance
Sample code ^a	Photo				
SUMW03A. US1.1		Hemispherical bowls with wide girth and plain in-turned rim	I.2.4.5	Medium compact fabric with white and dark inclusions, mica and steatite	Arabia
SUM08B. US162.104		Hemispherical bowls with wide girth and plain in-turned rim	I.2.4.5	Medium compact fabric with white and dark inclusions, mica and steatite	Arabia
SUM11A. US174.232 ^b		Lid-cum-bowl	I.5.1	Compact fabric with black and white inclusions of various size	India

TABLE 1 (Continued)




Samples from Sumhuram		Vessel shape	Vessel type	Macroscopic characteristics of the fabric	Provenance
Sample code ^a	Photo				
SUM09A. US297.2		Pots with out-turned bulging rim	I.1.1.8	Compact fabric with large amount of white, black inclusions and grit temper	India
SUM10C. US162.119		Fragment of bowl or dish	—	Compact fabric with white inclusions and mica (?)	India
SUM11A. US54.85		Globular jars with simple everted rim	II.1.18	Fine fabric with small amount of white inclusions	India

TABLE 1 (Continued)




Samples from Sumhuram		Vessel shape	Vessel type	Macroscopic characteristics of the fabric	Provenance
Sample code ^a	Photo				
SUM08A, US253.5		Pots with out-turned beaked or pointed rim	I.1.1.1	Medium compact fabric with small white and red inclusions	India
SUM10C, US174.79		Fragment of bowl or dish	—	Medium compact fabric with red inclusions, mica and quartz (?)	India
SUM03A, US133.9		Pots with out-turned rounded rim	I.1.1.2	Coarse fabric with large amount of black and white inclusions and mica	India

TABLE 1 (Continued)




Samples from Sumhuram		Vessel shape	Vessel type	Macroscopic characteristics of the fabric	Provenance
Sample code ^a	Photo				
SUM10A. US405.3		Pots with out-turned beaked or pointed rim	I.1.1.1	Medium compact fabric with small white and red inclusions	India
SUM10C. US174.104		Shallow bowl with rim horizontal in the upper part	I.2.1.3	Rice temper ware	India
SUM10A. US412.1		Pots with out-turned rounded rim	I.1.1.2	Coarse fabric with large amount of black and white inclusions and mica.	India

TABLE 1 (Continued)






Samples from Sumhuram		Vessel type	Macroscopic characteristics of the fabric	Provenance
Sample code ^a	Photo	Vessel shape		
SUM10C. US174.83		Lids-cum-bowl	Compact fabric with white inclusions of large size, dark inclusions and mica	India
SUM03B. US93.23		Jars with flaring neck and enlarged everted rim	Medium compact fabric with white and dark inclusions, mica and grit temper	India
SUM09B. US309.4		Lamps/lid with rounded bottom and reservoir inside	Compact fabric with white and grey inclusions	India

TABLE 1 (Continued)

Samples from Sumhuram		Vessel shape	Vessel type	Macroscopic characteristics of the fabric	Provenance
Sample code ^a	Photo				
SUM03B. US93.42		Jars with everted collared rim	II.1.1	Medium compact fabric with black and white inclusions	India
SUM08B. US275.4		Cooking pot	—	Unidentified fabric type	India

^aThe sample code is structured with site code, year of excavation, number of the stratigraphic unit, number of the sample (SUM, Sumhuram; IQM, Inqitat).

^bThe same sample is identified as SUM10C.US174.232 in Pavan (2017). In the specificity of the article, the sample keeps the Buffa (2019) coding and description, being the more recent of the two catalogues.

TABLE 1 (Continued)




Samples from Inqiat and its surroundings					
Sample code ^a	Photo	Vessel shape	Vessel type	Macroscopic characteristics of the fabric	Provenance
IQM16B.US35.8		Pot with a tenon, pierced lug	Shell ware	Coarse fabric with many grit and shell temper	Arabia
IQM18B. US119.5		Fragment of wall of a jar	Dot-in-circle ware	Compact fabric with some small inclusions	Arabia
IQM17A.US58.5		Jar with short and vertical neck and flat rim	Shell ware	Compact fabric with shell temper	Arabia

TABLE 1 (Continued)




Samples from Inqitat and its surroundings					
Sample code ^a	Photo	Vessel shape	Vessel type	Macroscopic characteristics of the fabric	Provenance
IQM17A.US58.8		Jar with out-turned pointed rim.	Mica ware	Fabric with red inclusions and mica tempered	Arabia
QM16B.US35.34		Storage jar (?)	Mica ware	Fabric rich in mica temper	Arabia
IQM16B.US35.35		Unidentified wall	Mica ware	Fabric rich in mica temper	Arabia

TABLE 1 (Continued)




Samples from Inqiat and its surroundings					
Sample code ^a	Photo	Vessel shape	Vessel type	Macroscopic characteristics of the fabric	Provenance
IQM16B. US35.33		Unidentified wall	Mica ware	Fabric rich in mica temper	Arabia
IQM16B. US35.32		Unidentified wall	Mica ware	Fabric rich in mica temper	Arabia
IQM16B.US30.6		Big globular jar	—	Compact fabric	India

TABLE 1 (Continued)




Samples from Inqitat and its surroundings					
Sample code ^a	Photo	Vessel shape	Vessel type	Macroscopic characteristics of the fabric	Provenance
IQM16B.US30.3		Storage jar with out-turned rim with internal groove in the upper part of the wall	—	Medium compact fabric	India
IQM17A.US35.16		Jar with out-turned rounded lip	—	Medium coarse fabric with red and white inclusions	India
IQM16B.US35.31		Unidentified wall	Red ware	Medium compact fabric with few small inclusions	Arabia

TABLE 1 (Continued)







Samples from Inqitat and its surroundings					
Sample code ^a	Photo	Vessel shape	Vessel type	Macroscopic characteristics of the fabric	Provenance
IQM17A. US35.18		Pot with out-turned rim	—	Fabric with red and white inclusions	India
IQM16B. US30.10		Fragment of wall of a storage container	—	Compact fabric	India
IQM18A.US80.3		Table jar with flaring neck and enlarged everted rim	—	Buff compact fabric	India

TABLE 1 (Continued)

Samples from Inqitat and its surroundings					
Sample code ^a	Photo	Vessel shape	Vessel type	Macroscopic characteristics of the fabric	Provenance
IQM16B.US35.9		Jar with short neck and simple everted rim	—	Fabric with white, black and red temper	India
IQM17B.US73.1		Fragment of wall of a storage container	—	Medium compact fabric	India
IQM16B.US23.13		Fragment of wall	Paddle impressed ware	Compact fabric	India

^aThe sample code is structured with site code, year of excavation, number of the stratigraphic unit, number of the sample (SUM, Sumhuram; IQM, Inqitat).

^bThe same sample is identified as SUM10C.US174.232 in Pavan (2017). In the specificity of the article, the sample keeps the Buffa (2019) coding and description, being the more recent of the two catalogues.

Optical microscopy

The thin sections were analysed by means of a polarized microscope (Leica DM 2500P) equipped with a mounted Leica MC170 HD camera and communicating with Leica Application Suite V 4.4 software. The presence of minerals and rock fragments as well as matrix characteristics, porosity and sorting, was described according to the scheme proposed by Quinn et al. (2013). The sphericity and dimensions of the grains were described using the terminology proposed by Adams et al. (1984).

Powder X-ray diffraction

PXRD was conducted on powdered samples using a Bruker AXS D8 Discovery X-ray diffractometer with Da Vinci design, a Cu K α source operating at 40 kV and 40 mA and a Lynxeye one-dimensional detector. The scans were run from 3° to 75° 2 θ , with 1 s for acquisition time and 0.05 2 θ step. PXRD allowed for mineralogical bulk analysis using the ICDD^{ix} databases and the software Diffrac.Suite provided by Bruker.

Inductively coupled plasma–mass spectrometry

ICP-MS analyses were conducted following the method used by Beltrame et al. (2019), which consists of three cycles of hotplate digestion of approximately 100 mg powdered sample in PFA Savillex beakers. The first digestion cycle was done by adding a mixture with 2 mL 47% HF (OPTIMA grade) and 0.5 mL of 65% HNO₃ (Suprapur grade) to the powdered sample, which were left to digest in the closed beakers on a hotplate at ~100°C for 48 h. After 48 h, the samples were dried by evaporation. However, the evaporation was not complete to avoid precipitation of the components and the formation of new stable compounds. Following evaporation, the second digestion cycle with 2 mL freshly made aqua regia was initialized. The mix was left on the hotplate at 100°C for 24 h. The following day, after evaporation, a final cycle of digestion targeting the organic compounds was conducted, with the addition of 2 mL pure HNO₃ (65%) at 100°C for 24 h. After drying the samples, the final solution for the trace elements was prepared by adding 1.6 mL HNO₃ (65%) and then filling with Milli-Q water to 50 mL. The aim was to reach a solution concentration of 2% HNO₃. For analysis of the major elements, the solutions were diluted 100-fold with 2% concentrated HNO₃. The final analysis was conducted on an Agilent 8800 ICP Triple Quad (ICP-QQQ). Prior to analysis, the equipment was calibrated with the tuning solution provided by Agilent Technologies. Moreover, a calibration curve was selected as the method for quantification of the analyses, which was prepared by the analysis of 10 differently concentrated solutions of Standard A: NHO₃ (2%); and Standard B: NHO₃ (2%) (from High Purity Standards). The concentrations reached were of 0, 5, 10, 20, 50, 100, 200, 400, 800 and 1600 ppb. The validity of the elemental quantification of the samples was verified by preparing triplicates of each sample. At the same time, the accuracy of the analysis was observed by preparing and running the certified reference materials AGV-2 and W-2a simultaneously on the samples. Experimental detection limits were performed by first measuring a 0 ppb solution in the acid matrix solution (HNO₃ at 2%) and then a 100 ppb solution in the same matrix of Standard A and Standard B in 11 replicates each. The quantification limits were determined as 10 times the detection limits. The results regarding major elements were then converted into oxides by stoichiometry and their concentration normalized to 100%. The trace elements were measured in ppm, and the rare earth element (REE) results were normalized to chondrite (Sun & McDonough, 1989). A limitation of the presented technique is the impossibility of directly measuring SiO₂ concentrations. Considering the importance of having

an indication of the SiO_2 quantification, its percentage was extrapolated by means of comparing the quantification of the major element oxides and the LOI weight data. The data were extracted by means of the difference between LOI results and the total percentage of the major oxides represented in the sample.

Scanning electron microscopy with energy-dispersive X-ray spectroscopy

Microanalysis and micro-imaging are crucial steps to enhance the comprehension of ceramic composition, as they allow for identification of the components that may remain undetectable by other methodologies due to their low concentrations or microscopic dimensions (Froh, 2004; Tite, 1991; Tite et al., 1982). The analysis was conducted with a variable-pressure Hitachi S3700N SEM instrument coupled with a Quantax EDS microanalysis system on the same thin sections previously studied by optical microscopy. The Quantax system was equipped with a Bruker Axs 5010 XFlash Silicon Drift Detector (129 eV spectral resolution at FWHM/MnK α). The SEM-EDS quantification was done using the software ESPRIT by Bruker. Operating conditions were as follows: backscattering mode (BSEM); 20 kV accelerating voltage; 10 mm working distance; 100 μA emission current; and 40 Pa pressure in the chamber. The major chemical elements recognized as making up the specific components within the sample matrix were converted into oxides by stoichiometry and normalized to 100%.

RESULTS

Optical microscopy

Analysis of the ceramic samples through optical microscopy highlights the diverse nature of the samples studied, resulting in their subdivision into eight different groups. This is based on a combination of textural and compositional features such as amount, nature, shape and dimension of inclusions and tempers, as well as matrix characteristics (Tables 2 and 3). The fabrics identified are shell-tempered (ST), shale-rich fabric (SF), talc-rich fabric (TF), basalt-rich fabric (BF), rice-tempered (RT), fine fabric (FF), medium-large inclusion in fine matrix (MLM) and shell- and sand-rich fabric (SSF).

The ST fabric is distinguishable by the moderate to abundant ($\sim 40\%$) presence of unsorted, angular shell fragments equal to or smaller than 0.5 mm, being of probable intentional addition. Other subordinate inclusions are limestone and quartz grains.

SF is mainly characterized by the presence of rounded shale clasts together with highly variable inclusions: well-preserved shells and shell fragments, calcite, micas, quartz, feldspars and hornblende amphibole with preserved euhedral forms were identified. The variability of types and dimensions of the inclusions suggests a very poor preparation of the raw material prior to ceramic production.


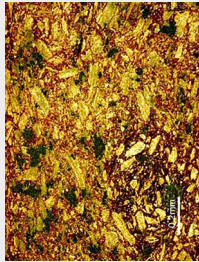
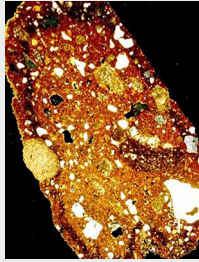
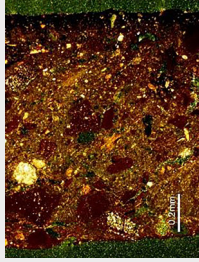
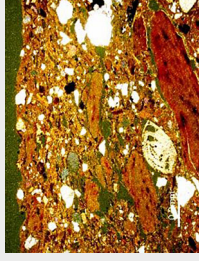
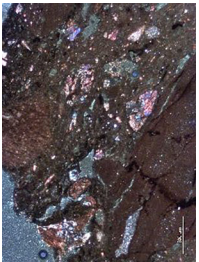
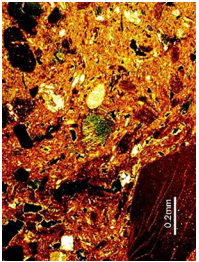
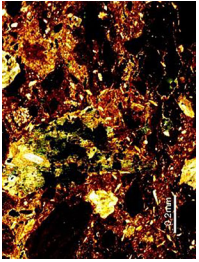

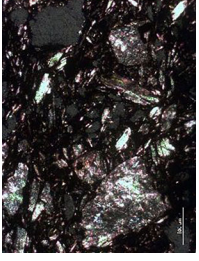
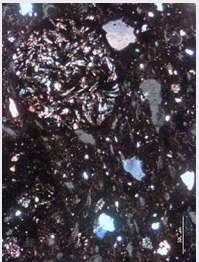
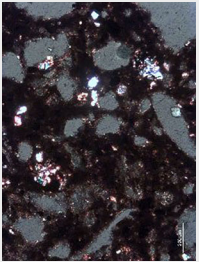
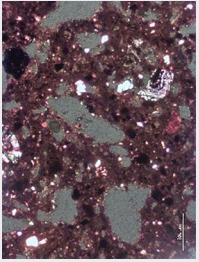
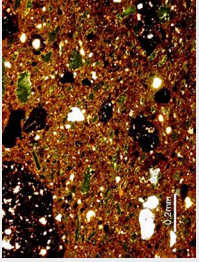
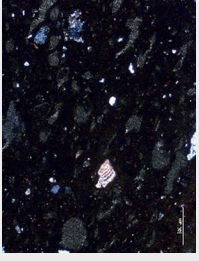
TF can be divided petrographically into two subgroups. Both subgroups (TF-1 and TF-2) are characterized by the presence of talc, although in different amounts. TF-1, together with unsorted angular talc-schist grains ($\sim 10\%$), also includes an important amount ($\sim 20\%$) of large shale grains and traces of calcite, quartz and opaques. On the other hand, TF-2 is composed mainly of angular talc-schist grains ($\sim 40\%$) of variable dimensions associated with very few quartz and chemogenic sedimentary rock inclusions, possibly chert. The general composition of the TF-2 subgroup suggests quite an important degree of raw material preparation, with talc grains being of probable intentional addition.

BF is the group most represented across all samples. It exhibits the presence of basalt inclusions as a key characteristic. However, basalt grains are few, and their dimensions and

TABLE 2 Schematic presentation of the identified fabric groups and of their main characteristics identified by the different techniques.

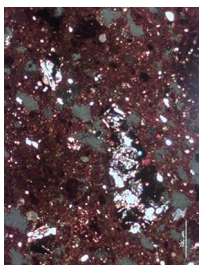
Group	Sample		Main characteristic	
Shell-tempered (ST)	<ul style="list-style-type: none"> • IQM16B.US35.8 • IQM17A.US58.5 	<ul style="list-style-type: none"> • IQM18B.US119.5 	Angular shell fragments used as temper	Quartz and limestone inclusions
Shale-rich fabric (SF)	<ul style="list-style-type: none"> • IQM17A.US58.8 • IQM16B.US35.34 	<ul style="list-style-type: none"> • IQM16B.US35.35 	<ul style="list-style-type: none"> • Rich in medium–large and rounded shale grains • Unsorted inclusions 	<ul style="list-style-type: none"> • Identification of shell fragments, calcite crystals, micas, quartz, feldspars and amphiboles as inclusions
Talc-rich fabric (TF)	<ul style="list-style-type: none"> • IQM16B.US35.33 (TF-1) • IQM16B.US35.32 (TF-1) 	<ul style="list-style-type: none"> • SUMW03A.US1.1 (TF-2) • SUM08B.US162.104 (TF-2) 	<ul style="list-style-type: none"> • Talc-schist grains • TF-2 with unsorted talc crystals as temper 	<ul style="list-style-type: none"> • Large variety in inclusions within TF-1 • Shale grains identified in TF-1
Basalt-rich fabric (BF)	<ul style="list-style-type: none"> • IQM16B.US30.6 • IQM117A.US35.16 • IQM16B.US30.3 • IQM17A.US35.18 • IQM16B.US35.31 	<ul style="list-style-type: none"> • SUM11A.US174.232 • SUM09A.US297.2 • SUM08B.US275.4 • SUM11A.US54.85 	<ul style="list-style-type: none"> • Variable concentration and dimensions of basalt grains • Plagioclases, quartz, and pyroxenes as major inclusions 	<ul style="list-style-type: none"> • Micas, hematite, anatase (commonly identifiable) • Presence of rice husks and volcanic glass in some samples
Rice-tempered (RT)	<ul style="list-style-type: none"> • SUM10C.US174.83 • SUM10A.US412.1 	<ul style="list-style-type: none"> • SUM10C.US174.104 	<ul style="list-style-type: none"> • Rice husks used as temper • Abundant pores resulting from vegetal temper loss during firing • Presence of small, rounded basalt grains 	<ul style="list-style-type: none"> • Small to extremely small and rounded quartz, crystalline calcite and opaques as inclusions
Fine fabric (FF)	<ul style="list-style-type: none"> • SUM10C.US162.119 • IQM16B.US30.10 	<ul style="list-style-type: none"> • IQM18A.US80.3 	<ul style="list-style-type: none"> • Very fine matrix composition with limited inclusions • Inclusions of various types: quartz, plagioclase and micas 	<ul style="list-style-type: none"> • IQM18A.US80.3 presents an extremely fine matrix • SUM10C.US162.119 with bone fragments and Fe-rich slip different from the Ca-rich core
Medium-large inclusions in fine matrix (MLM)	<ul style="list-style-type: none"> • SUM10A.US405.3 • SUM03A.US133.9 • IQM16B.US35.9 • IQM17B.US73.1 	<ul style="list-style-type: none"> • IQM16B.US23.13 • SUM08A.US253.2 • SUM10C.US174.79 	<ul style="list-style-type: none"> • Medium–large temper grains (between 100 and 500 μm) • Majority of inclusion composed by quartz and feldspars 	<ul style="list-style-type: none"> • The grog is generally fine and homogeneous
Shell- and sand-rich fabric (SSF)	<ul style="list-style-type: none"> • SUM03B.US93.23 • SUM03B.US93.42 	<ul style="list-style-type: none"> • SUM09B.US309.4 	<ul style="list-style-type: none"> • Quartz grains and recrystallized limestones as other major inclusions • Sandy matrix 	<ul style="list-style-type: none"> • Common presence of feldspars and micas • Rich in well-rounded shell fragments

TABLE 3 XPL images presenting the composition of each sample analysed. The pictures have a 0.2 mm scale.

				
IQM16B.US35.8 (ST)	IQM17A.US58.5 (ST)	IQM18B.US119.5 (ST)	IQM17A.US58.8 (SF)	IQM16B.US35.34 (SF)
				
IQM16B.US35.35 (SF)	IQM16B.US35.33 (TF-1)	IQM16B.US35.32 (TF-1)	SUMW03A.US1.1 (TF-2)	SUM08B.US162.104 (TF-2)
				
IQM16B.US30.6 (BF)	IQM17A.US35.16 (BF)	IQM16B.US30.3 (BF)	IQM17A.US35.18 (BF)	IQM16B.US35.31 (BF)

(Continues)

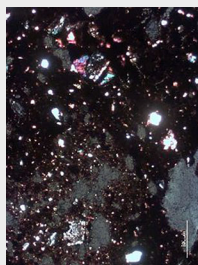
TABLE 3 (Continued)



SUM11A.US174.232 (BF)^a



SUM09A.US297.2 (BF)^a



SUM08B.US275.4 (BF)^a



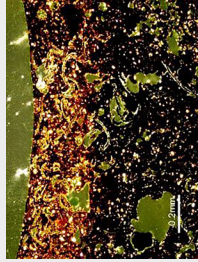
SUM11A.US54.85 (BF)^a



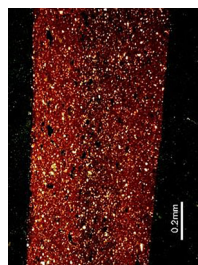
SUM10C.US174.83 (RT)



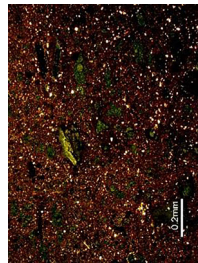
SUM10A.US412.1 (RT)



SUM10C.US174.104 (RT)



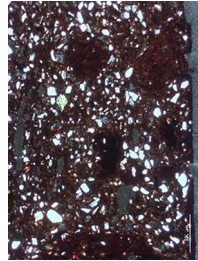
SUM10C.US162.119 (FF)



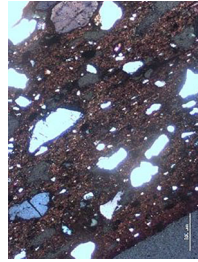
IQM16B.US30.10 (FF)



IQM18A.US80.3 (FF)^a


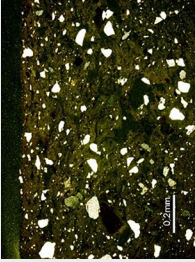
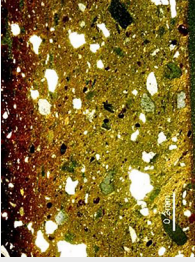
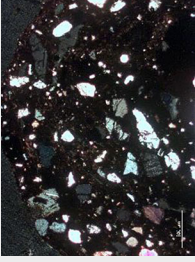
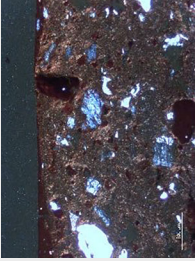
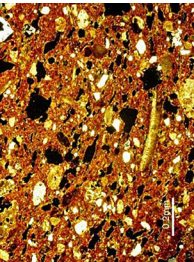
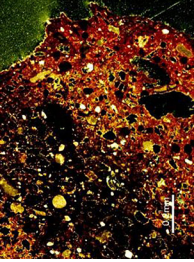
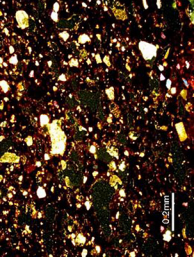


SUM10A.US405.3 (MLM)^a



SUM03A.US133.9 (MLM)^a

TABLE 3 (Continued)

 <p>IQM16B.US35.9 (MLM)</p>	 <p>IQM17B.US73.1 (MLM)</p>	 <p>IQM16B.US23.13 (MLM)</p>	 <p>SUM08A.US253.5 (MLM)^a</p>	 <p>SUM10C.US174.79 (MLM)^a</p>
 <p>SUM03B.US93.23 (SSF)</p>	 <p>SUM03B.US93.42 (SSF)</p>	 <p>SUM09B.US309.4 (SSF)</p>		

Abbreviations: BF, basalt-rich fabric; FF, fine fabric; MLM, medium-large inclusions in fine matrix; RT, rice-tempered; SF, shale-rich fabric; SSF, shell- and sand-rich fabric; ST, shell-tempered; TF, talc-rich fabric.

^aPictures with scale 500 µm.

roundness are not consistent across the samples. Despite the variability, the presence of basalt in all the samples strongly suggests a common geographical/geological provenance. A large variability of poorly sorted inclusions—that is, quartz, feldspars, opaques, pyroxene, calcite, olivine and rice husks—were also identified, with variations in the association of such components across the different samples of this group.

The RT fabric group also presents traces of basalt grains. The distinction between BF and RT groups lies in the evident use of rice husks as intentionally added temper in the latter (reaching 30–40%), while it is only sporadically identifiable in the former. The RT fabric is characterized by a high degree of porosity connected to the degradation of rice husks, which left undisputable imprints on the material surrounding them, as mentioned by several other authors (Lischi, Odelli, et al., 2020; Tomber et al., 2011). Together with rice husks and rare basalt grains, a limited number of small quartz, calcite and opaque grains was observed through optical microscopy.

The FF group's main characteristic is the fine material and remarkable quality of ceramic production. The few recognizable inclusions are muscovite and quartz or feldspar grains. The fabric is generally non-porous and, in one of the samples, there was evidence of a slip.

MLM is the second most represented group. In this group, the samples share the similar characteristic of presenting homogeneously large grains as inclusions within a generally fine and homogeneous matrix. In particular, most of such large inclusion grains are quartz (~30%). Still, it is also possible to recognize, at subordinate amounts, the presence of feldspars, calcite, opaque phases, micas, pyroxene and detrital sedimentary rock grains, possibly sandstones. Within this petrographic group, significant variability is mainly related to the dimension and angularity of the larger inclusions and the concentration of specific minerals.

Lastly, SSF presents some well-rounded shell fragments and well-rounded spirititic limestone grains within a coarse sandy matrix. Within the fabric, it is also possible to recognize some quartz grains and opaques.

Powder X-ray diffraction

The general mineralogical composition was obtained using PXRD on powdered samples. The results highlight the important differences between the fabric groups and the invariability within the groups, validating the previous petrographic features. A summary of diffractogram interpretation is presented in Table 4.

Although the mineralogical composition shows important variations between the different fabric groups, quartz is always present and is usually one of the most abundant temper phases. Calcite represents the major mineral phase in the ST and SSF groups, corresponding to the presence of shell fragments. Calcite is also abundant within SF group, sharing similar concentrations with plagioclase and amphibole.

The TF sample diffractograms reflect the high amount of talc, but a distinction can be noticed between TF-1 and TF-2 due to the higher variability in the composition of the TF-1 group. In fact, together with talc, quartz and amphiboles, calcite and plagioclases are also present in this group. Otherwise, TF-2 diffractograms show only some traces of quartz, calcite and micas, beyond talc.

In addition to the very high quartz and plagioclase concentration registered in the BF diffractograms, hematite and pyroxene are also present in significant amounts, congruent with the basaltic nature of the temper. Furthermore, the most important characteristic recognizable is the very limited presence of calcite and the relatively constant presence of hematite. A similar mineralogical composition is found in the diffractograms of the RT groups, underlining the similarity between the two groups as mentioned before.

TABLE 4 XRD results for each sample grouped in the following order: ST, SF, BF, RT, FF, MLM and SSF. The phases connected to the firing temperature of the ceramic are separated from the other phases and highlighted by *.

Sample name	Q	C	Do	Pl	K-F	H	M	OI	Py	Am	An
IQM16B.US35.8	x	xxxx	-	-	-	-	xx	-	-	-	-
IQM17A.US58.5	xx	xxxx	-	-	-	-	x	-	-	-	-
IQM18B.US119.5	xxx	xxx	-	-	-	-	x	-	-	-	-
IQM17A.US58.8	xx	xxx	-	x	-	-	x	-	-	xx	-
IQM16B.US35.34	xx	x	-	xx	-	-	xx	-	-	xx	-
IQM16B.US35.35	xx	x	-	xx	-	x	-	-	-	xxx	-
IQM16B.US35.33	xx	x	-	x	-	-	-	-	-	xx	-
IQM16B.US35.32	x	x	-	x	-	-	-	-	-	xx	-
SUMW03A.US1.1	x	+	-	-	-	-	x	-	-	-	-
SUM08B.US162.104	+	+	-	-	-	+	+	-	-	-	-
IQM16B.US35.31	xx	x	x	xxx	-	+	x	-	-	-	x
IQM16B.US30.6	xx	-	x	xx	-	x	-	-	-	x	x
IQM17A.US35.16	xxx	x	-	xx	-	x	-	-	-	-	x
IQM16B.US30.3	xx	-	x	xx	-	x	xx	-	x	-	x
IQM17A.US35.18	xx	x	-	xxx	-	x	-	-	xx	-	x
SUM11A.US174.232	xxx	x	-	xx	-	x	xx	-	-	-	+
SUM09A.US297.2	xx	x	-	xxx	-	x	x	-	x	-	-
SUM08B.US275.4	xx	+	-	xx	x	x	x	x	-	-	-
SUM11A.US54.85	xxx	x	-	xx	-	x	x	-	x	-	-
SUM10A.US412.1	xxx	+	-	xx	-	-	x	-	x	-	-
SUM10C.US174.104	xxx	+	-	xx	xx	-	xx	x	x	-	-
SUM10C.US174.83	xxx	+	-	xx	x	x	x	-	-	-	-
IQM16B.US30.10	xxx	x	-	xx	-	+	xx	-	-	-	-
SUM10C.US162.119	xxx	x	-	xx	xx	+	xx	-	-	-	-
IQM18A.US80.3	xxx	x	-	x	x	+	xx	-	-	-	-
SUM10A.US405.3	xx	-	-	xx	xx	-	x	-	-	xx	-
IQM16B.US35.9	xxx	-	x	x	xx	-	xx	-	-	-	+

TABLE 4 (Continued)

Sample name	Q	C	Do	Pl	K-F	H	M	Ol	Py	Am	An
IQM17B.US73.1	xxxx	+	-	x	xx	-	-	-	-	-	-
MLM	xxx	+	-	xx	xx	-	-	-	x	-	-
SUM08A.US253.5	xx	+	-	xx	xx	-	x	-	-	x	-
SUM10C.US174.79	xxx	-	-	x	xx	-	xx	-	x	-	-
SUM03A.US133.9	xxx	-	-	-	xx	+	x	-	-	-	-
SUM03B.US93.23	xxx	xx	-	x	x	-	xx	-	-	-	-
SSF	xx	xxx	-	x	x	+	x	-	x	-	-
SUM03B.US93.42	xx	xx	-	x	x	-	xx	-	-	-	-

TABLE 4 (Continued)

Ta	Gy	Ze	Ch	Ka	Go	Si	Rh	Sp ^a	Cr ^a	Di ^a	Mu ^a	Ge ^a	Wo ^a
-	-	-	-	-	-	-	-	-	-	x	-	-	-
ST	-	-	-	-	-	-	-	-	-	x	-	-	-
-	-	-	-	-	-	-	-	-	-	x	+	-	-
-	-	-	xx	-	-	-	+	-	-	-	x	-	-
SF	-	-	-	-	-	-	-	-	-	x	-	-	-
-	-	-	-	-	-	-	-	-	-	x	-	x	-
xxx	-	-	xx	-	-	-	-	-	-	x	-	-	-
TF-1	xxx	x	-	x	-	-	-	-	-	+	-	-	-
xxxx	-	+	x	-	-	-	-	-	-	-	-	-	-
TF-2	xxxx	+	-	-	-	-	-	-	-	-	-	-	-
-	-	-	-	-	-	-	-	-	-	x	-	-	-
-	x	-	-	-	-	-	-	-	-	x	-	-	-
-	-	-	-	-	-	-	-	-	-	x	x	-	-
-	xx	-	-	-	-	-	-	-	-	x	-	-	-
BF	-	-	-	-	-	-	-	-	-	-	-	-	-
-	-	-	-	-	-	-	-	-	-	x	-	-	-
-	+	-	-	-	-	-	+	-	-	-	-	-	-

TABLE 4 (Continued)

	Ta	Gy	Ze	Ch	Ka	Go	Si	Rh	Sp ^a	Cr ^a	Di ^a	Mu ^a	Ge ^a	Wo ^a
	-	-	-	-	-	-	-	-	x	-	x	-	+	-
	-	-	-	-	-	-	-	-	-	+	x	-	-	-
	-	-	-	-	-	-	-	-	-	-	-	-	-	x
RT	-	-	-	-	-	-	-	-	-	-	-	-	-	-
	-	-	-	-	-	-	-	-	-	-	x	x	-	-
	-	xx	-	-	-	-	-	-	-	-	x	x	+	-
FF	-	-	-	-	-	-	-	-	-	+	x	x	x	-
	-	-	-	-	-	-	-	-	-	-	x	x	-	-
	-	-	-	-	-	-	-	-	-	-	-	-	-	-
	-	-	-	-	-	x	x	-	-	-	x	-	-	x
	-	-	-	-	-	x	-	-	-	-	-	x	-	-
MLM	-	-	-	-	-	-	-	-	-	-	x	-	-	-
	-	-	-	-	-	-	-	-	-	-	-	-	-	-
	-	-	-	-	-	-	-	-	-	-	-	x	-	-
	-	-	-	-	-	-	-	-	-	-	-	x	-	-
	-	-	-	-	-	-	-	-	-	-	-	x	+	x
SSF	-	+	-	-	-	-	-	-	-	-	x	x	x	-
	-	-	-	-	-	-	-	-	-	-	x	x	x	-

Note: xxxx = between 70% and 100%; xxx = between 40% and 70%; xx = between 10% and 40%; x = less than 10%; + = present; - = absent.

Am, amphiboles; C, calcite; Ch, chlorite; Cr, cristobalite; Di, diopside; Do, dolomite; Ge, gehlenite; Go, goethite; Gy, gypsum; H, hematite; Ka, kaolinite; K-F, K-feldspars; M, micas; Mu, mullite; Ol, olivine; Pl, plagioclase; Py, pyroxene; Q, quartz; Rh, rhodomite; Si, sillimanite; Sp, spinel; Ta, talc; Wo, wollastonite; Ze, zeolite.

^aRelated to ceramic firing temperature.

MLM-group diffractograms show a different mineralogy, represented by the highest quartz concentration of all samples, together with K-feldspar and plagioclase.

Lastly, the FF group presents a mineralogical composition that includes quartz, plagioclase, K-feldspar and mica. Such a composition is not remarkably different from the other groups, especially from groups BF, MLM and RT. The distinction of the FF group from the rest of the sample was mainly based on texture rather than mineralogical composition.

PXRD analysis also allowed for the recognition of phases that were impossible to identify through optical microscopy. Some of them could be important for future firing process analyses of these ceramics. In particular, the FF and SSF groups are characterized by mullite and gehlenite, not observed on RT samples. The remaining fabric groups show only sporadic examples of mullite, gehlenite, spinel and wollastonite, without any evidence of consistent group-related characteristic composition.

Inductively coupled plasma–mass spectrometry

Obtaining elementary chemical composition data aimed at validating the separation into groups made previously and possibly finding chemical tracers to identify provenance. Detailed oxide values are presented in Table 5, while the trace element results obtained with ICP-MS are presented in Table 6.

As presented in Figure 2, the higher variability is for Al_2O_3 and CaO, which generally match with previously defined petrographic groups, allowing for their individualization. Moreover, within each defined petrographic group, the major elemental composition exhibits a similar global elemental signature (Figure 3).

The high CaO concentration (36.9–44.9 wt%) in ST samples is a distinguishing feature. This matches with the higher amounts of calcite identified by PXRD and the shell fragments identified by optical microscopy. Lower enrichment in CaO (\sim 17.0–17.7 wt%) is presented in the SSF group, which also presents high Al_2O_3 contents (10.1–11.6 wt%).

The main characteristic of the SF group is the relatively high Al_2O_3 concentrations (17.0–18.4 wt%), representing not only the clayish nature of the paste but also indicating the presence of shale inclusions. Relative variability in CaO can be related to the irregular presence of shell fragments within the different samples.

MgO concentration is crucial for distinguishing between the TF groups and is directly related to the amount of talc used as a temper. TF-1 exhibits a lower MgO concentration (6.6–8.9 wt%) and higher CaO content (7.9–8.8 wt%) compared to TF-2 (MgO: 17.2–24.6 wt%; CaO: 1.8–2.2 wt%). The lower MgO concentration in TF-1, along with its higher CaO content compared to TF-2, results from the lower concentration of talc fragments and the higher quantity of inclusions of various nature within the composition.

The BF group is characterized by an Al_2O_3 concentration that ranges between 12.6 and 22.6 wt%. The variations in Al_2O_3 , noticeable also in the concentration of Fe_2O_3 (7.5–15.3 wt%), are to be considered indicative of the variable ratio between the inclusions and the paste of the samples.

The RT samples, similar to the BF ones, show a high concentration of Al_2O_3 (12.3–13.2 wt%) and Fe_2O_3 (9.3–10.2 wt%). Estimation of the SiO_2 concentrations in the RT samples shows the highest values, probably related to SiO_2 enrichment caused by the addition of rice husks.

Similarly to RT, the FF group, with a small number of inclusions, also shows high Al_2O_3 , CaO and Fe_2O_3 concentrations. Chemically, the main difference between RT and FF is the higher CaO concentration (7.6–10.4 wt%) in FF compared with RT (3.2–3.8 wt%).

Lastly, MLM reaches the highest concentration of Al_2O_3 (18.6–26.3 wt%) of all samples. Such a composition agrees with the higher feldspar amount (K-feldspar \pm plagioclase) as an inclusion.

TABLE 5 Major elemental composition (wt%) per sample.

Group	Sample name	Na ₂ O	MgO	Al ₂ O ₃	P ₂ O ₅	K ₂ O	CaO	TiO ₂	MnO	Fe ₂ O ₃	^a SiO ₂
ST	IQM16B.US35.8	0.30	2.12	6.83	0.04	1.20	36.93	0.37	0.07	3.99	48.16
	IQM17A.US58.5	0.30	1.62	4.88	0.17	1.09	44.96	0.23	0.03	2.85	43.88
	IQM18B.US119.5	0.27	2.31	4.24	0.08	0.48	38.74	0.37	0.06	2.89	50.56
SF	IQM17A.US58.8	1.14	4.14	17.43	0.12	2.34	12.06	0.97	0.05	5.93	55.82
	IQM16B.US35.34	2.05	5.33	18.45	1.08	2.93	9.04	1.27	0.07	7.67	52.10
	IQM16B.US35.35	1.58	5.11	17.06	0.14	2.30	15.81	0.89	0.08	7.31	49.72
TF-1	IQM16B.US35.33	1.74	6.61	13.69	0.19	2.80	7.96	0.93	0.07	7.54	58.47
	IQM16B.US35.32	1.88	8.89	12.30	0.28	2.47	8.83	0.83	0.09	8.45	55.99
TF-2	SUMW03A.US1.1	1.00	24.59	8.13	0.10	1.87	1.83	0.44	0.07	6.98	54.99
	SUM08B.US162.104	0.69	17.16	11.35	0.16	1.64	2.17	0.67	0.08	9.03	57.05
BF	IQM16B.US35.31	1.45	2.60	22.60	0.38	1.23	5.09	3.84	0.10	7.79	54.93
	IQM16B.US30.6	1.86	2.71	21.62	0.34	1.37	4.14	3.20	0.11	7.71	56.94
	IQM17A.US35.16	1.43	2.54	22.49	0.36	1.16	5.00	3.75	0.09	7.49	55.69
	IQM16B.US30.3	2.00	3.07	18.11	0.42	1.45	6.33	2.99	0.10	7.59	57.96
	IQM17A.US35.18	1.62	3.36	19.08	0.32	1.38	4.58	3.30	0.10	8.30	57.96
	SUM11A.US174.232	1.78	3.61	12.64	0.70	2.37	4.05	2.61	0.27	12.99	58.99
	SUM09A.US297.2	1.80	2.75	19.50	0.12	0.50	5.98	2.01	0.17	12.62	54.55
	SUM08B.US275.4	1.93	2.92	13.81	0.34	2.02	3.69	3.25	0.21	15.26	56.56
SUM11A.US54.85	1.86	4.29	14.59	0.26	1.99	5.45	1.63	0.13	10.21	59.58	

(Continues)

TABLE 5 (Continued)

Group	Sample name	Na ₂ O	MgO	Al ₂ O ₃	P ₂ O ₅	K ₂ O	CaO	TiO ₂	MnO	Fe ₂ O ₃	^a SiO ₂
RT	SUM10A.US412.1	1.80	2.21	13.24	0.48	2.19	3.21	1.88	0.13	10.21	64.64
	SUM10C.US174.104	2.01	2.21	12.34	0.43	2.69	3.72	1.88	0.15	9.86	64.71
	SUM10C.US174.83	1.54	2.46	12.28	0.64	2.43	3.84	1.90	0.13	9.26	65.52
FF	IQM16B.US30.10	1.51	3.90	14.30	0.42	2.88	10.45	1.09	0.15	8.57	56.74
	SUM10C.US162.119	1.19	3.51	14.66	0.31	2.95	7.68	1.05	0.10	7.51	61.04
	IQM18A.US80.3	2.25	4.76	14.76	0.18	2.98	8.74	0.84	0.12	6.69	58.69
MLM	SUM10A.US405.3	2.57	1.73	19.21	0.23	3.37	2.25	1.10	0.06	8.58	60.90
	IQM16B.US35.9	0.94	0.80	25.44	0.09	1.99	1.81	1.25	0.02	4.60	63.06
	IQM17B.US73.1	0.49	0.62	26.31	0.09	1.12	1.07	2.36	0.03	3.50	64.41
	IQM16B.US23.13	1.09	0.96	24.15	0.14	2.61	1.71	1.11	0.02	4.30	63.91
	SUM08A.US253.5	2.76	1.24	18.59	0.16	3.53	2.29	1.04	0.02	8.04	62.32
	SUM10C.US174.79	1.59	0.63	22.28	0.42	3.08	1.91	1.38	0.02	6.54	62.17
	SUM03A.US133.9	1.32	0.78	21.13	0.33	2.17	1.25	1.98	0.02	9.10	61.94
	SUM03B.US93.23	1.03	1.92	10.92	0.31	2.26	17.32	0.78	0.08	5.65	59.74
SSF	SUM09B.US309.4	1.01	2.30	10.13	0.67	2.50	17.73	0.66	0.10	5.60	59.31
	SUM03B.US93.42	1.02	2.29	11.60	0.25	2.80	17.02	0.64	0.05	6.01	58.31

^aSiO₂ values resulting from indirect calculations and quantifications. The data were extracted by means of the difference between LOI results and the total percentage that the major oxides represent of the sample.

TABLE 6 Trace elements composition per sample (ppm).

Groups	Sample name	Sc	V	Cr	Co	Ni	Cu	Zn	Ga	Ge
ST	IQM16B.US35.8	6,93	102,16	117,61	17,77	77,74	18,96	32,07	8,03	1,33
	IQM17A.US58.5	6,93	74,29	81,70	9,73	48,54	13,02	29,05	6,03	1,12
	IQM18B.US119.5	5,28	45,32	43,41	5,09	20,31	6,83	34,68	6,77	1,35
SF	IQM17A.US58.8	14,62	101,73	95,84	19,38	55,57	13,76	45,95	16,95	2,18
	IQM16B.US35.34	19,89	150,11	140,63	21,72	62,27	29,12	78,64	20,57	2,87
	IQM16B.US35.35	14,84	96,96	93,65	25,76	72,42	31,41	66,13	18,53	2,55
TF-1	IQM16B.US35.33	15,73	130,96	121,92	31,67	135,77	22,12	76,94	19,38	3,16
	IQM16B.US35.32	14,13	101,90	333,03	44,94	228,10	22,28	88,56	20,14	3,51
TF-2	SUMW03A.US1.1	12,65	91,76	1,027,27	47,54	989,66	27,79	84,13	11,81	4,03
	SUM08B.US162.104	13,04	195,98	1,217,04	41,54	1,017,99	33,05	110,34	14,49	3,57
BF	IQM16B.US35.31	82,55	257,95	551,48	20,33	67,93	88,84	73,35	32,52	5,25
	IQM16B.US30.6	77,71	286,81	483,30	24,50	70,10	85,87	78,22	35,43	5,41
	IQM17A.US35.16	85,69	253,54	551,40	21,16	71,02	87,97	73,21	34,32	5,44
RT	IQM16B.US30.3	75,28	260,64	426,45	26,83	74,14	92,33	79,53	35,60	5,67
	IQM17A.US35.18	77,02	242,74	450,61	29,72	79,70	96,60	80,63	34,15	5,82
	SUM11A.US174.232	26,12	255,32	1,070,10	60,21	374,75	121,00	125,84	17,10	3,17
RT	SUM09A.US297.2	18,01	258,65	128,04	37,71	85,15	129,47	88,79	24,29	2,92
	SUM08B.US275.4	29,62	364,41	599,69	53,06	130,26	134,56	128,06	20,08	3,39
	SUM11A.US54.85	22,12	243,04	140,47	30,31	72,19	93,08	80,66	21,45	3,10
	SUM10A.US412.1	25,09	219,06	107,17	28,32	62,56	142,23	100,69	19,60	3,44
	SUM10C.US174.104	26,66	200,99	113,65	35,47	71,60	122,25	98,38	20,94	4,16
SUM10C.US174.83	22,61	217,98	110,84	28,94	58,06	120,95	104,41	18,17	3,07	

TABLE 6 (Continued)

Groups	Sample name	Sc	V	Cr	Co	Ni	Cu	Zn	Ga	Ge
FF	IQM16B.US30.10	19,15	134,80	149,88	21,51	97,04	53,47	99,01	18,71	
	SUM10C.US162.119	16,55	154,90	158,25	22,66	113,44	79,01	103,57	20,58	3,27
	IQM18A.US80.3	19,47	153,40	165,09	24,05	115,10	49,90	86,20	20,36	3,12
MLM	SUM10A.US405.3	19,14	148,72	175,26	22,19	75,92	49,83	98,02	27,55	4,56
	IQM16B.US35.9	20,79	103,94	150,40	11,72	58,13	31,75	79,00	31,03	4,10
	IQM17B.US73.1	19,42	88,60	196,54	12,21	75,13	25,59	74,31	33,85	4,51
	IQM16B.US23.13	20,91	113,04	147,79	13,62	60,70	22,24	84,92	34,69	4,42
	SUM08A.US253.5	21,16	125,37	172,21	11,94	61,21	40,80	66,04	28,65	4,69
	SUM10C.US174.79	22,01	163,49	157,65	14,70	80,37	42,48	87,30	34,66	4,61
SSF	SUM03A.US133.9	18,01	136,18	143,13	11,02	48,46	32,58	106,88	33,60	5,72
	SUM03B.US93.23	14,31	111,55	134,60	14,46	56,27	27,72	88,51	14,11	2,42
	SUM09B.US309.4	14,49	112,21	193,46	16,03	76,14	32,24	72,92	13,40	2,43
	SUM03B.US93.42	12,84	111,97	121,36	13,54	73,63	33,66	80,55	15,46	2,63
Groups	Sample name	La	Ce	Pr	Nd	Sm	Eu	Gd	Tb	Dy
ST	IQM16B.US35.8	14,73	34,80	4,02	14,58	3,75	0,65	2,60	0,39	2,22
	IQM17A.US58.5	11,26	26,85	2,67	10,67	2,42	0,52	1,86	0,28	1,64
	IQM18B.US119.5	12,59	26,75	3,20	7,84	2,99	0,71	2,09	0,31	2,02
SF	IQM17A.US58.8	16,85	37,07	4,60	16,77	4,40	0,92	3,31	0,54	3,42
	IQM16B.US35.34	22,96	51,71	6,39	23,28	6,06	1,23	4,11	0,63	3,77
	IQM16B.US35.35	21,72	48,39	6,00	21,67	6,09	1,09	4,39	0,73	4,80
TF-1	IQM16B.US35.33	22,15	50,22	6,22	25,52	5,23	1,18	4,48	0,69	4,33
	IQM16B.US35.32	25,00	56,66	7,22	30,35	6,06	1,38	5,34	0,82	5,25

TABLE 6 (Continued)

Groups	Sample name	Sc	V	Cr	Co	Ni	Cu	Zn	Ga	Ge
TF-2	SUMW03A.US1.1	11,22	28,15	2,33	8,86	1,93	0,45	1,60	0,27	
	SUM08B.US162.104	22,36	49,14	5,42	18,57	3,86	0,78	3,52	0,54	3,53
BF	IQM16B.US35.31	18,04	45,78	6,30	25,44	9,04	2,38	5,43	0,96	6,36
	IQM16B.US30.6	18,59	54,79	7,50	30,15	10,57	2,36	6,84	1,27	8,02
	IQM17A.US35.16	18,75	46,52	6,56	24,51	9,32	2,32	5,58	1,00	6,60
	IQM16B.US30.3	17,11	40,51	7,18	32,88	9,23	2,55	6,89	1,18	7,44
	IQM17A.US35.18	20,00	53,94	8,07	36,31	9,73	2,87	7,56	1,27	8,01
	SUM11A.US174.232	23,05	52,51	6,30	25,66	6,10	1,47	5,46	0,84	5,10
	SUM09A.US297.2	11,61	29,56	3,78	16,75	4,59	1,38	4,19	0,69	4,36
	SUM08B.US975.4	16,59	42,12	4,93	18,89	5,27	1,42	4,68	0,78	5,01
	SUM11A.US54.85	26,25	57,95	6,67	24,55	5,40	1,34	5,19	0,78	4,92
	SUM10A.US412.1	26,56	54,39	6,73	26,37	6,24	1,41	5,32	0,86	5,25
RT	SUM10C.US174.104	28,80	61,86	7,21	24,53	5,54	1,48	5,18	0,78	4,91
	SUM10C.US174.83	24,32	51,92	6,16	23,31	5,19	1,31	4,93	0,76	4,77
FF	IQM16B.US30.10	25,58	55,32	6,29	20,26	5,59	1,30	4,10	0,63	3,94
	SUM10C.US162.119	29,86	64,47	7,40	24,42	5,39	1,15	4,87	0,71	4,33
MLM	IQM18A.US80.3	30,71	64,24	7,43	28,24	5,32	1,23	4,69	0,68	4,04
	SUM10A.US405.3	63,08	128,33	13,54	47,56	8,77	2,05	6,78	0,87	4,72
	IQM16B.US35.9	47,14	107,73	11,14	39,09	9,61	1,94	6,67	0,99	6,16
	IQM17B.US73.1	65,11	135,25	14,12	49,72	10,57	1,64	6,71	0,88	5,04
	IQM16B.US23.13	56,72	124,69	13,20	49,75	9,14	1,91	7,53	1,03	6,03
	SUM08A.US253.5	63,45	128,39	13,54	50,10	7,72	2,50	6,50	0,79	4,25
SSF	SUM10C.US174.79	52,53	115,10	12,09	42,81	6,89	2,19	6,32	0,82	4,71
	SUM03A.US133.9	85,42	193,67	21,42	78,09	12,63	1,32	9,90	1,10	5,27
	SUM03B.US93.23	24,74	50,41	6,13	22,73	5,17	0,98	4,31	0,63	3,81
	SUM09B.US309.4	24,21	49,88	5,78	19,20	4,65	0,94	4,14	0,62	3,85
	SUM03B.US93.42	21,82	45,99	5,42	20,46	4,14	0,77	3,40	0,55	3,13

TABLE 6 (Continued)

Groups	Rb	Sr	Y	Zr	Nb	Cd	Sn	Sb	Cs	Ba
ST	76,56	389,49	10,99	41,98	5,79	0,23	1,36	0,36	4,65	273,11
	44,12	428,56	9,73	33,28	4,26	0,48	0,84	0,23	2,17	91,63
	17,66	588,02	10,84	43,26	6,26	0,42	0,84	0,21	0,88	128,62
SF	47,73	369,59	16,76	83,38	10,45	0,71	1,69	0,22	3,08	248,18
	75,97	546,40	16,51	80,25	11,62	0,43	2,75	0,23	4,36	321,68
	57,93	287,84	24,92	118,38	10,82	0,39	2,12	0,26	2,65	306,61
TF-1	53,85	199,88	23,63	135,57	11,27	0,36	2,12	0,25	2,27	356,29
	52,01	173,51	29,78	141,53	10,50	0,37	2,27	0,26	1,92	340,65
	40,73	61,94	9,37	50,80	8,56	0,11	1,28	1,00	1,82	136,10
TF-2	55,86	1,039,72	19,54	75,96	12,60	0,19	1,92	2,39	3,99	95,14
	21,20	412,53	22,48	292,83	25,94	0,37	3,22	0,17	0,52	372,43
	21,36	330,61	26,07	249,72	22,27	0,33	2,97	0,14	0,56	123,31
BF	20,99	343,17	22,91	295,41	25,62	0,38	3,27	0,15	0,52	324,14
	18,15	265,04	25,57	240,34	22,27	0,32	2,84	0,13	0,54	129,18
	18,80	331,85	27,00	254,25	23,72	0,36	3,10	0,18	0,54	385,61
RT	35,54	217,59	24,80	120,62	13,75	0,27	2,45	0,62	2,08	190,23
	11,64	193,36	21,17	60,24	10,97	0,13	2,28	0,23	0,72	117,18
	30,57	243,89	23,88	122,08	14,35	0,26	1,91	0,40	0,97	265,10
RT	75,15	249,49	24,98	98,43	15,71	0,16	2,56	0,56	4,28	277,90
	59,66	162,68	27,28	72,69	15,74	0,27	2,84	0,52	2,84	278,51
	65,85	260,38	27,29	120,68	16,16	0,41	3,31	0,34	2,32	305,56
	61,35	275,21	24,76	93,26	15,20	0,19	3,57	0,38	2,09	306,08

TABLE 6 (Continued)

Groups	Rb	Sr	Y	Zr	Nb	Cd	Sn	Sb	Cs	Ba
FF	99,88	445,95	20,59	80,14	13,21	0,25	2,81	0,50	6,83	
	118,89	226,37	23,09	61,39	16,24	0,23	3,13	0,75	9,33	285,27
	111,90	302,23	22,07	86,62	14,35	0,35	3,02	0,49	8,47	426,96
MLM	69,96	366,09	21,97	8,82	14,97	0,17	2,50	0,45	1,78	1,452,53
	101,18	273,15	28,23	55,40	19,95	0,15	2,23	0,20	2,05	709,30
	68,55	113,88	21,71	86,77	39,76	0,16	4,00	0,42	4,06	429,89
SSF	105,85	237,34	28,44	58,00	21,14	0,23	2,20	0,20	2,30	617,94
	82,57	456,31	21,81	46,39	14,37	0,13	2,26	0,24	1,57	1,550,12
	37,77	238,95	21,96	54,25	20,01	0,14	3,20	0,27	1,47	1,174,41
SSF	86,80	69,35	20,32	41,89	45,28	0,12	2,44	0,48	2,17	432,15
	76,80	1,474,40	20,16	64,46	10,28	0,57	2,20	0,49	6,29	169,13
	81,90	324,51	22,14	30,47	10,09	0,27	2,08	0,57	6,32	205,59
ST	102,91	3,201,64	15,94	16,36	10,26	0,41	2,83	0,63	9,94	222,26
	0,43	1,09	0,17	0,95	0,15	1,25	9,40	0,15	5,10	1,38
	0,31	0,78	0,12	0,83	0,11	1,01	12,61	0,10	4,14	1,02
SF	0,40	0,93	0,16	0,99	0,13	1,27	7,66	0,02	3,43	2,22
	0,69	1,74	0,29	1,68	0,25	2,49	9,68	0,05	4,20	1,44
	0,73	1,72	0,29	1,60	0,24	2,53	11,47	0,03	4,78	1,66
TF-1	0,98	2,33	0,40	2,25	0,33	3,46	16,08	0,02	5,14	1,60
	0,86	2,25	0,36	2,48	0,36	3,55	11,78	0,14	4,93	1,73
	1,04	2,56	0,42	2,83	0,38	3,57	8,01	0,15	5,22	1,27
TF-2	0,34	0,86	0,14	0,97	0,13	1,43	11,27	0,04	4,65	1,46
	0,72	1,87	0,31	1,87	0,30	2,47	26,78	0,09	7,12	2,44

TABLE 6 (Continued)

Groups	Rb	Sr	Y	Zr	Nb	Cd	Sn	Sb	Cs	Ba
BF	1,16	2,59	0,45	2,60	0,35	7,45	6,81	0,04	7,98	1,60
	1,47	3,44	0,55	3,04	0,44	6,69	6,36	0,06	7,04	1,55
	1,21	2,70	0,47	2,58	0,36	7,52	6,22	0,06	7,76	1,64
	1,34	3,14	0,49	3,33	0,44	5,80	7,44	0,09	6,27	1,45
	1,43	3,33	0,52	3,53	0,45	6,26	8,71	0,07	6,86	1,45
	0,99	2,53	0,37	2,09	0,33	3,48	160,59	0,08	6,96	1,21
	0,87	2,26	0,33	1,87	0,29	1,80	11,29	0,03	1,74	0,58
	0,96	2,53	0,36	2,07	0,32	4,08	19,00	0,01	3,57	0,85
	0,96	2,28	0,37	2,12	0,33	2,77	22,93	0,01	8,50	1,44
	1,03	2,76	0,39	2,20	0,34	3,16	69,71	0,05	9,42	1,42
RT	0,93	2,18	0,35	2,25	0,28	2,89	38,31	0,14	8,58	1,28
	0,93	2,24	0,35	2,04	0,32	2,61	40,89	0,08	7,78	1,25
	0,78	1,86	0,31	1,77	0,25	2,32	16,35	0,11	9,58	1,63
	0,85	2,16	0,34	1,98	0,31	2,23	70,81	0,25	11,92	1,79
FF	0,79	1,97	0,31	2,13	0,29	2,24	24,05	0,05	12,69	1,78
	0,87	2,29	0,31	1,81	0,28	1,53	242,39	0,03	13,91	0,96
MLM	1,18	2,69	0,46	2,56	0,36	1,69	36,30	0,16	14,94	2,69
	0,92	2,12	0,35	2,05	0,27	2,54	38,41	0,20	25,42	4,52
	1,14	2,77	0,43	2,91	0,40	1,59	48,41	0,28	19,18	2,77
	0,77	1,85	0,27	1,77	0,22	1,43	58,11	0,09	13,43	1,62
	0,86	2,04	0,31	2,01	0,24	1,72	87,40	0,09	14,51	1,27
	0,91	2,15	0,33	2,01	0,31	2,01	42,88	0,17	46,13	4,95
SSF	0,75	2,08	0,29	1,73	0,27	2,14	15,11	0,15	10,50	1,68
	0,77	2,06	0,30	1,76	0,28	1,61	29,11	0,10	9,26	1,43
	0,60	1,65	0,25	1,47	0,23	1,80	17,29	0,13	10,52	1,90

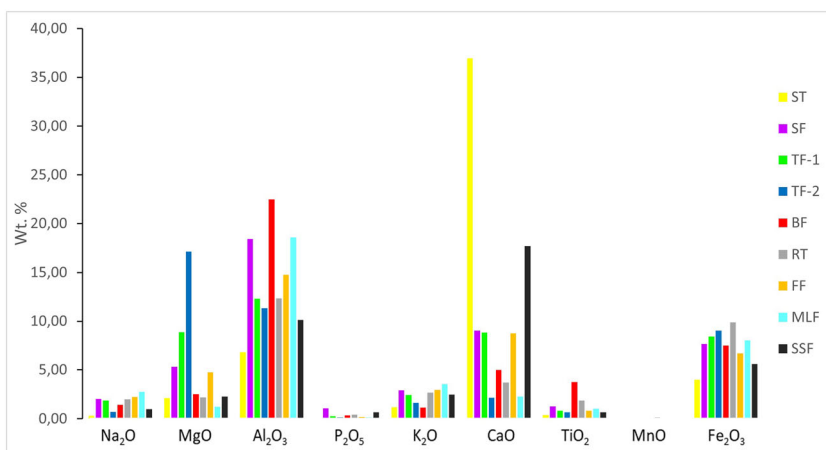


FIGURE 2 Major element (wt%) comparison of one representative sample per group. BF, basalt-rich fabric; FF, fine fabric; MLM, medium-large inclusions in fine matrix; RT, rice-tempered; SF, shale-rich fabric; SSF, shell- and sand-rich fabric; ST, shell-tempered; TF, talc-rich fabric.

When the samples are plotted on the ternary diagram of Heimann and Maggetti (2019) (Figure 4) based on their Al_2O_3 , SiO_2 and $\text{CaO} + \text{MgO}$ values, most of the groups become readily identifiable. Additionally, incorporating in the plotting the distinction between Arabic and Indian materials recognized by Pavan (2017) and Lischi et al. (2022) results in a clear distinction between the groups. A clear separation in provenance is identifiable with the Arabic samples, characterized by an enrichment of MgO and CaO concentrations as a consequence of the presence of, respectively, talc and shells in the paste.

A similar distinction is visible when conducting principal component analyses (Figure 5) using the four components discussed above.^x The Arabic and Indian materials are separated, except for the similar behaviour of FF and SF groups. ST stands out from the rest of the groups, while the TF group is clearly split into the two subgroups TF-1 and TF-2. Lastly, the SSF group identified as Indian (Lischi, 2019) overlaps with the Arabic groups, as also visible in Figure 4.

Regarding trace elements, there is a greater dispersion in the data obtained with, in general, no clear relationship with the considered petrographic groups. Nevertheless, Ni or Cr is enriched in the TF and BF samples (Table 6), matching the presence of talc-schist and basaltic inclusions, respectively. On the other hand, the enrichment of Ba in the MLM samples (Table 6) correlates with the higher content of K-feldspar and biotite.

As argued so far, trace elements can be strongly influenced by small inclusions present in the ceramic, leading to signal variability within the same fabric groups. Comparably, REE^{xi} concentrations (Table 6) also show no clear geochemical signature. The only noticeable remarks from the study of REE values are that the highest REE content was found in the MLM samples and that the highest La^*/Lu^* ratio occurs in the same group. This suggests the presence of REE-rich mineral phases (e.g., monazite, allanite) within MLM not detectable by PXRD or optical microscopy.



FIGURE 3 Major oxide composition plots of the different groups. The images should be combined into one single one, with groups being from left to right and top to bottom in the following order: ST (yellow), SF (purple), TF (green and blue), BF (red), RT (grey), FF (green), MLM (light blue) and SSF (brown).

Scanning electron microscopy with energy-dispersive X-ray spectroscopy

Microanalyses using SEM-EDS were conducted to corroborate some textural and compositional features previously obtained through OM, with the aim of comparing the chemical composition of inclusions and to complete the description of the fabric characteristics (Table 7).

The ST group's main characteristic is the unsorted shell fragments used as temper. Their CaCO₃ composition was confirmed through SEM-EDS and noticed as being occasionally associated with SiO₂.

Within the SF group, it was possible to confirm the presence of Mg-rich amphiboles (hornblende; Figure 6) and shale grains identified by the enrichment of Al, Si and K. The overlapping of Ca and P elemental map distribution indicates the presence of bone fragments.

Observations through SEM-EDS within TF-2 confirmed the presence of abundant talc grains (Mg enrichment) and iron oxide grains.

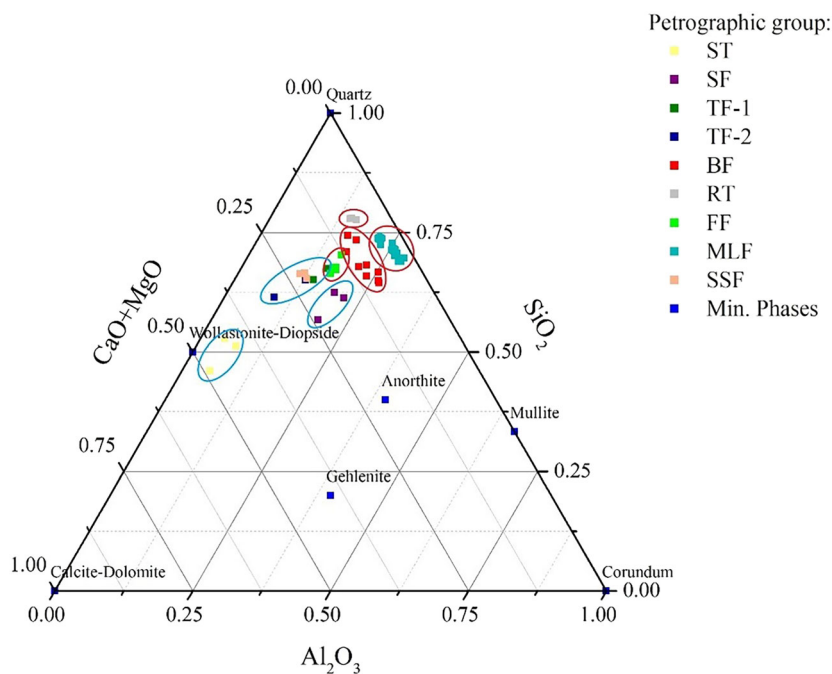


FIGURE 4 Ternary diagram (after Heimann & Maggetti, 2019) of major oxides in correspondence of Al_2O_3 , SiO_2 and $\text{CaO} + \text{MgO}$ with stylistically identified Arabic in blue circles and Indian in red circles. BF, basalt-rich fabric; FF, fine fabric; MLM, medium-large inclusions in fine matrix; RT, rice-tempered; SF, shale-rich fabric; SSF, sand- and shell-rich fabric; ST, shell-tempered; TF, talc-rich fabric.

On BF samples, occasional traces of rice husks (Si-rich) were found and the presence of basalt grains and, in some samples, of volcanic glass were confirmed.

As mentioned before, the RT group includes a few basalt grains, confirmed by means of SEM-EDS. The presence of well-preserved rice husks was also confirmed through texture and the Si-rich composition. The elemental analysis through EDS shows that the pyroxenes found in the RT paste are distinct from those analysed in the BF group (Figure 7). This observation suggests that the raw material originates from distinct basaltic rock sources. However, the composition of the pyroxenes, whether present as grains within the paste of the BF sample or in basalt inclusions within the same sample, remains consistent.

The FF group samples, when observed by means of SEM-EDS, highlight some differences within the group. Sample IQM18A.US80.3 demonstrates an extremely fine matrix with hardly any inclusion. On the other hand, sample SUM10C.US162.119 results in very diversified minute inclusions, among which bone fragments were also recognizable. Furthermore, sample SUM10C.US162.119 presents a slip layer rich in Fe covering the Ca-rich composition of the ceramic body, a surface treatment not observed on the other FF samples. Analyses related to MLM confirmed the major role of quartz grains and K-feldspar as inclusions.

Lastly, the analysis of SSF confirmed the characteristics previously presented: shell fragments, which differ from the fragments in ST because they are more rounded and lacking Si in addition to Ca. It also confirmed rounded sparite limestones and some rounded quartz grains.

The elemental composition of the paste shows some dispersion across different samples considering CaO , SiO_2 and Al_2O_3 concentrations (Figure 8). Such variations in paste composition can also be seen within the MLM group. The lack of a strong chemical signature within the paste compositions of the groups is also noticeable.

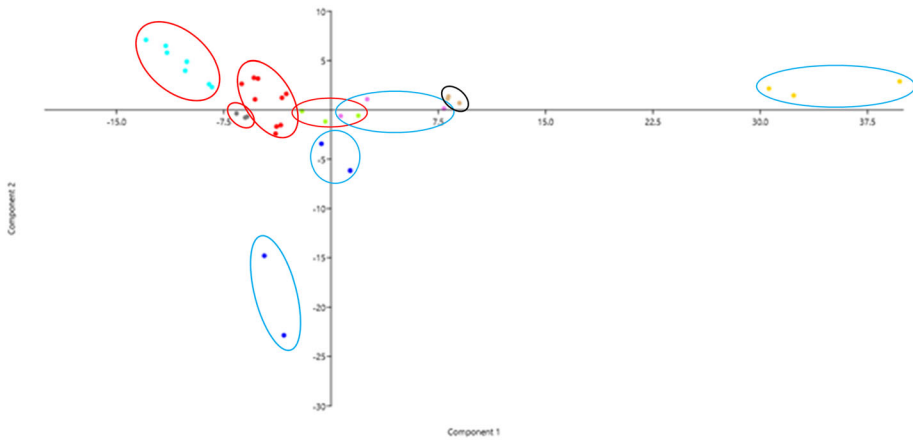


FIGURE 5 Principal component analyses of Al_2O_3 , SiO_2 and $\text{CaO} + \text{MgO}$, stylistically identifying Arabic provenance in blue circles and Indian provenance in red circles. ST: yellow; SF: violet; TF: blue; BF: red; RT: grey; FF: green; MLM: light blue; SSF: brown.

DISCUSSION

The main objective of this research is to understand how and to what extent the archaeometric study can help with recognizing the geological and chemical fingerprints that are instrumental in grouping and identifying the provenance of the ceramics involved in the trade connections in the Indian Ocean. The following discussion presents the provenance identification, but, as a consequence of the methodology-testing nature of the study, this is to be considered a preliminary result that is in need of further study, especially considering the limited number of samples analysed compared to the dimensions of the geographic region considered.

The use of a multi-analytical approach reveals a very complex provenance panorama, despite the small sample group. The identification of eight petrographic groups suggests a very dynamic and complex trade system, which can be mapped with well-detailed geological information about potential sources of raw material (Table 8).

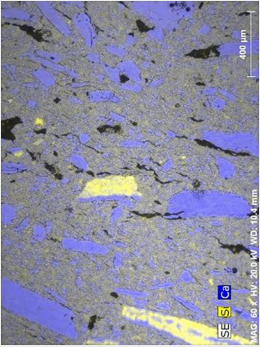
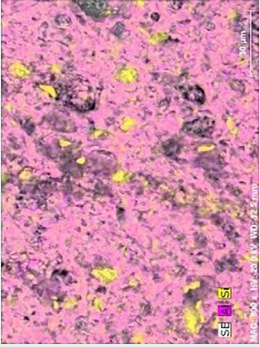
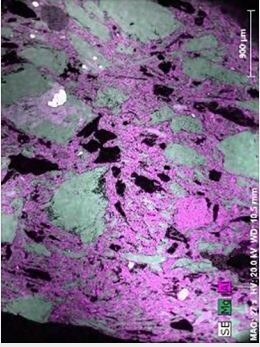
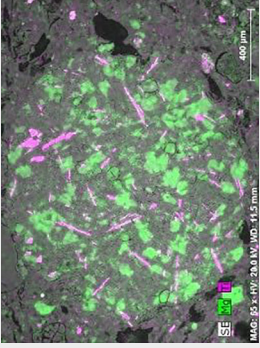
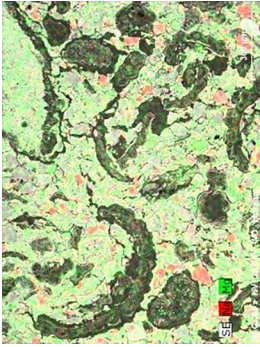
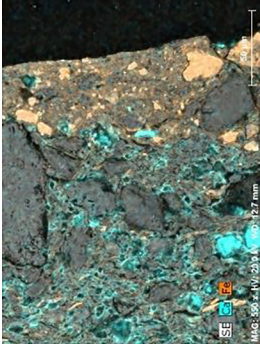
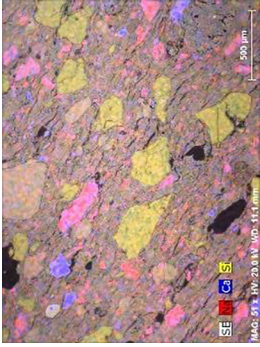
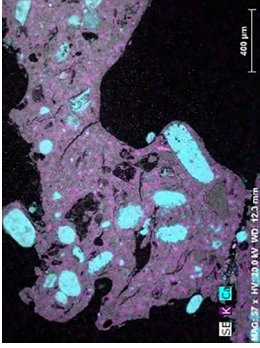
The plotting of the samples according to major element ratios (Figures 4 and 5) shows that the samples tend to cluster according to the archaeometric groups and that samples identified as Indian are clustered separated from those identified as Arabic artefacts (Lischi, 2022; Pavan, 2017).

As expected, when comparing areas such as the Arabian and Indian peninsulas, a significant variability of geological features is identified. However, not all the data obtained from the analysis can be directly compared to specific geological formations. In fact, some can be representative of a technological or cultural trait. Therefore, when possible, a direct comparison with archaeological materials of known origins is also made (Lischi, Pavan, & Fusaro, 2020; Maritan et al., 2007; Pallecchi & Pavan, 2011; Reddy, 2015).

The ST group stands out from all other groups for its CaO-rich (Figure 4) composition related to the strong presence of shell fragments used as a temper. Despite the lack of geological fingerprints within the fabric, the use of shell fragments as intentionally added temper is described as part of the ceramic tradition of the Dhofar region (Lischi, Pavan, & Fusaro, 2020; Pallecchi & Pavan, 2011; Reddy, 2015) (Figure 9), a peculiarity that is common to many coastal areas. It is therefore possible that production is local, but, in the absence of geological fingerprints, we cannot be certain of it.

The other samples included in the Arabic definition are the members of the SF and TF group. It has been noted that the SF group contains, as its most characteristic components,

TABLE 7 BSE images of the different groups with elemental mapping.

	<p>BSE image of ST group with the distribution of Si (yellow) and Ca (blue) both composing shell fragments</p>
	<p>BSE image of shale grain in SF group with the distribution of Al (pink: paste) and Si (yellow: quartz grains)</p>
	<p>BSE image of TF group with the distribution of Mg (green: talc) and Al (pink: paste)</p>
	<p>BSE image of basalt grain in BF with the distribution of Mg (green: pyroxene) and Ti (pink: oxide)</p>
	<p>BSE image of RT group with the rice husk imprints and the distribution of Mg (green: paste) and Na (red: plagioclase)</p>
	<p>BSE image of FF group with the distribution of Ca (blue: pores, bone fragments and plagioclase) concentrated in the inner body and Fe (orange: micas) concentrated on the surface</p>
	<p>BSE image of MLM group with the distribution of Na (red: feldspar), Ca (blue: amphiboles) and Si (yellow: quartz)</p>
	<p>BSE image of SFF group with the distribution of K (purple: paste) and Ca (blue: calcitic shell)</p>

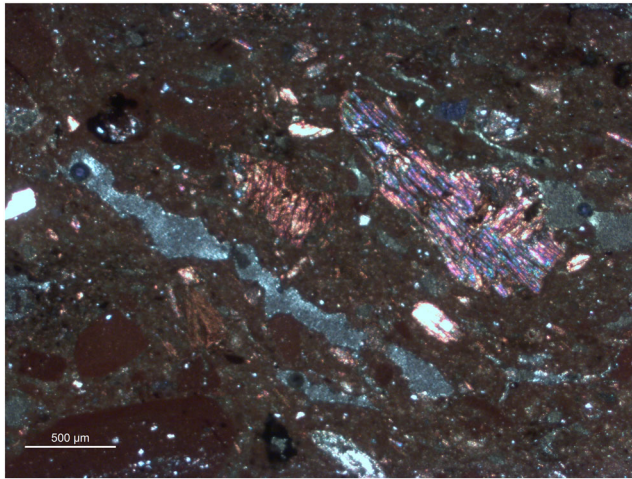


FIGURE 6 XPL image presenting the composition of sample IQM16B.US35.35 member of SF group. Image showing an example of hornblende.

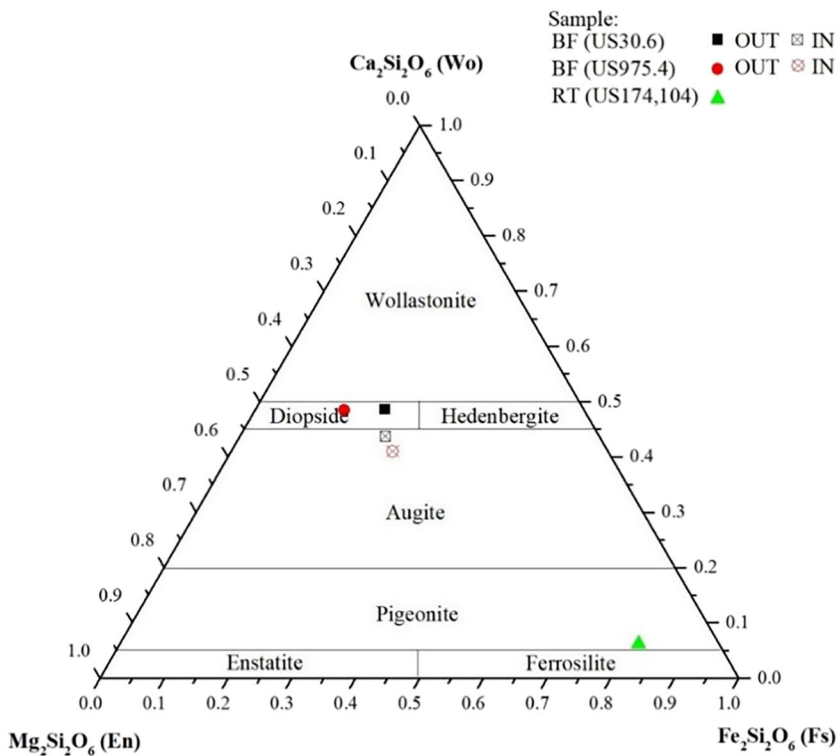


FIGURE 7 Ternary diagram of pyroxenes from BF samples and RT samples. The comparison is also between pyroxene located within basalt grains (crossed empty symbols) and single-pyroxene grains (full-coloured symbols), both within BF samples (after Heimann & Maggetti, 2019).

large shale grains, euhedral amphibole crystals and shells. The variability of temper refers to a varied geological origin (sedimentary and igneous/metamorphic for shales and amphibole,

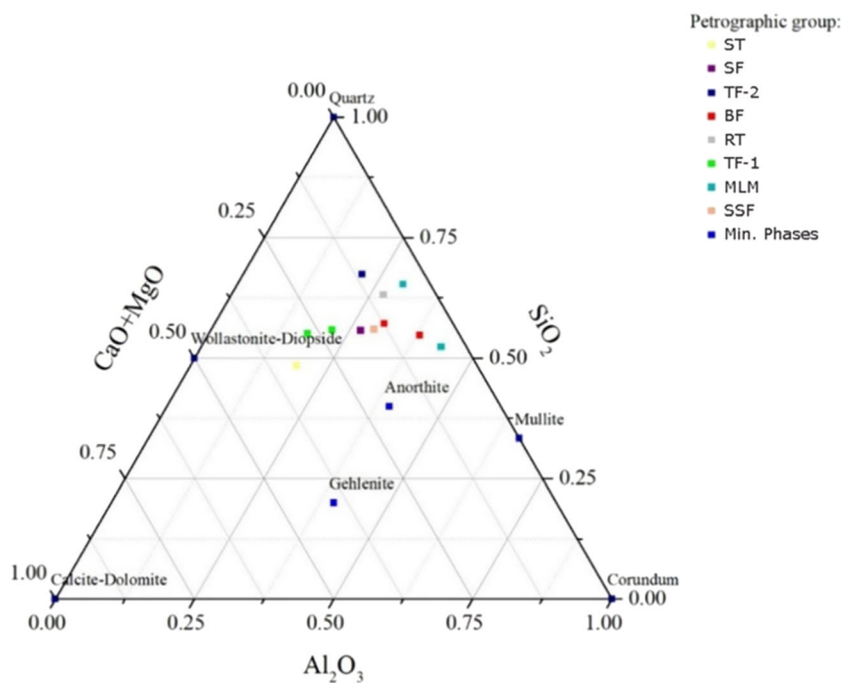


FIGURE 8 Ternary plot (after Heimann & Maggetti, 2019) representing the comparison of the matrix according to CaO + MgO, SiO₂ and Al₂O₃ (wt%). BF, basalt-rich fabric; FF, fine fabric; MLM, medium-large inclusions in fine matrix; RT, rice-tempered; SF, shale-rich fabric; SSF, shell- and sand-rich fabric; ST, shell-tempered; TF, talc-rich fabric.

respectively), although they were probably collected in the same way as the ST group: in coastal or estuarine environments, given the presence of complete shells. Moreover, the limestone-rich geology of Dhofar would not fit the description of the composition but, on the other hand, points to the west (Yemen) and north (Northern Oman) of the peninsula. There is a greater lithological variability that could explain the association of materials so distinct in their geological origin. From Figure 4, it is possible to notice how TF samples reflect the presence of talc in their higher MgO values. Talc is geologically relatable to the metamorphism of ultramafic parental rocks, which is characteristic of both the Yemenite Sarawat mountains and the northern Oman Al Hajar mountains. Of the two possible sources of talc, the Yemenite one represents the strongest candidate when the important economic and cultural connections between Sumhuram and the south Arabian Hadramawt kingdom are taken into account (Pavan, 2017). However, to exclude the possible Omani origin of the TF group, the REE patterns of the TF samples were compared (Figure 10) with those of archaeological talc stoneware published by Magee et al. (2005) from UAE (United Arab Emirates), which shares the Al Hajar mountains with Oman. The comparison between ceramic material and stoneware is not straightforward, but the extremely high concentration of talc-schist inclusions in the TF-2 samples can be considered as sufficient justification for the comparison. Taking into consideration the differences in nature of the materials analysed, the comparison between the TF-2 samples and data from Magee et al. (2005) shows a clear mismatch, which discards the hypothesis of a possible south-eastern Arabian origin of the TF raw materials. Due to the absence of references, similar comparisons between southwestern Arabian archaeological material and the samples studied in this paper have not been possible so far. However, if we consider the strong cultural and economic bonds between the city of Sumhuram and the south Arabian kingdoms as well as the mismatch

TABLE 8 Schematized presentation of the main characteristics (selected in relation to sample characteristics) of the different geological areas in the southern Arabian peninsula (Khalifa, 1988; Powers et al., 1966; Zerboni et al., 2020) and in the Indian subcontinent (Pandey et al., 2017; Wadia, 1919).

Geological area	Characteristics
West Yemen area	<ul style="list-style-type: none"> • Igneous plateau • Volcanic layers • In the north in contact with sedimentary layers • In the south, presence of contact metamorphic formations with talc presence • The metamorphic layers are covered by shale, limestone and sandstones layers
Hadramawt region	<ul style="list-style-type: none"> • Limestone plateau
Jabel Qara range	<ul style="list-style-type: none"> • Uplifted limestone • Karstic phenomena
Salalah plain	<ul style="list-style-type: none"> • Alluvial plain (fluvial erosion of the Jabel Qara range) • Sedimentary bedrock • Marls, limestones, dolomites, sandstones and breccia limestone outcrops
Rub'al Khali basin	<ul style="list-style-type: none"> • Aeolian sand desert
Omani mountain range	<ul style="list-style-type: none"> • Igneous (including Semail ophiolite) and metamorphic regions (with talc presence) • Salt formations • In the south these formations are covered by clastic and chemical marine layers • The southern end is composed by a limestone plateau
Himalayan ridge	<ul style="list-style-type: none"> • Uplifted marine deposits • Limestone, sandstone and fossiliferous layers
Alluvial plains of North India	<ul style="list-style-type: none"> • Alluvial deposition of eroded Himalayan geology • Inclusions of erosion of material from Central India
Deccan trap	<ul style="list-style-type: none"> • Igneous plateau • Basalt and volcanic glass
South India and Sri Lanka	<ul style="list-style-type: none"> • Landmasses that were never submerged • Coarsely grained metamorphic rocks (granite, granulose to schist-like gneisses) • Presence of sedimentary layers resulting from bedrock erosion
East Indian coastline	<ul style="list-style-type: none"> • Uplifted marine floor • Fluvial depositions of eroded material from the south Indian or the Deccan trap geological formations

previously presented, it is possible to argue in favour of a southwestern Arabian origin of the TF samples (Figure 10). Additionally, considering the similar chemical composition (both bulk composition, from ICP-MS analysis, and paste-specific composition, from SEM-EDS) of SF and TF-1, the common presence of shale grains and amphiboles, it is possible to hypothesize a southwestern Arabian origin of the SF group as well (Figure 10), in the absence of better data and comparable archaeological material. With such a possible identification of the SF group provenance, the ST fabric group is left as the only possibly locally produced one of the eight different fabric groups identified.

The other fabrics represented in Figures 4 and 5 are identified as Indian. However, as for the Arabic materials, the Indian materials are also separated into diverse fabric groups, of which the BF group is the most abundant. This group is characterized by the presence of basalt grains, which is indicative of the igneous nature of its geological origins, and by the presence of some rice husks among the inclusions, which, as discussed later, can be considered as tracing the production to South Asia. It must be mentioned, however, that rice husks were also found within some torpedo jars produced in Susa, where rice cultivation is attested from the first century CE (Lischi, Odelli, et al., 2020). The examples presented by Lischi, Odelli, et al. (2020), however, lack the presence of basalt inclusions, making the comparison between them and both the BF and RT groups ineffective. The Deccan Traps igneous geological area is located on the

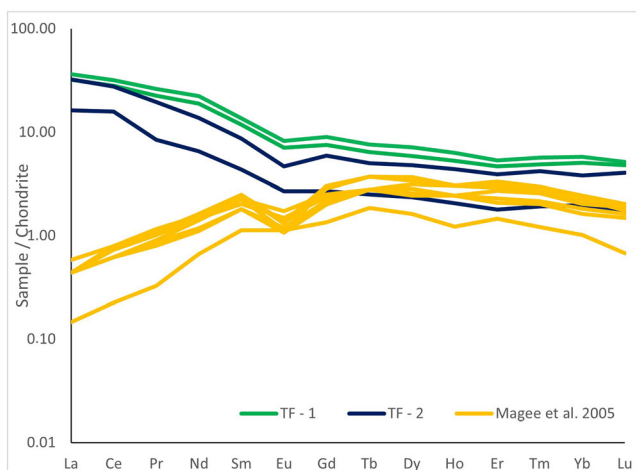


FIGURE 9 Comparison between REE patterns from TF samples (green TF-1 and blue TF-2) and from stoneware samples from UAE in yellow (Magee et al., 2005). Samples normalized to chondrite (Sun & McDonough, 1989).

Indian subcontinent's west/northwest side and is characterized by the presence of basalt layers. Despite the lack of direct comparison, both the presence of basalt and rice husks within the BF group and the Deccan Traps being the major source of basalt in the Indian subcontinent suggest a western Indian origin for the BF samples (Figure 10).

A similar argument can be proposed for the RT group, which includes rice husks as temper and small basalt grains as inclusions. However, it was possible to compare the RT samples with archaeological material published by Tomber et al. (2011) from sites like Kuda, Dhatva, Kamrej and Baroda in the Gujarat region along the northernmost coastal exposure of the Deccan Traps. The composition of the fabric (e.g., the presence of rice husks and basalts) of the published ceramics is very similar to that of the RT samples. Moreover, those authors characterize the ceramics presented as a homemade product and identify the use of rice as indicative of Gujarat as the area of production. The direct comparability between the RT samples with those presented by Tomber et al. (2011) also indicate the Gujarat region as the sourcing for the RT samples (Figure 10).

In Figure 4, the FF samples partially overlap with samples from the BF group. As mentioned before, the main characteristic of the FF group is the relatively high CaO concentration, which agrees with the calcite presence identified by PXRD. The identification of calcite suggests a non-igneous raw material, justifying the separation of FF samples from BF samples, and indicates a firing temperature of lower than 700°C (Maritan et al., 2009).

The characteristics defining the FF group, however, are not effective in identifying a specific geological formation. On the other hand, archaeological material originating from northeastern India (most probably from the Bay of Bengal), excavated from different sites spread around the southeastern Indian state of Tamil Nadu, included samples that display similar petrographic characteristics to those of the FF group (Odelli et al., 2020), indicating a possible northern Indian provenance for the FF group (Figure 10). However, despite it being a fascinating hypothesis, such a possible direction of trade needs to be further verified.

The MLM group, individualized by petrographic characteristics, is also established through major elements of chemical composition (Figures 4 and 5). It is characterized by the inclusions of large crystals (mainly quartz, but also feldspars, amphiboles and calcite) with well-preserved crystal faces. These associations of angular and faced silicate crystals can be indicative of proximal granitic parental material. Petrographic comparisons were possible with archaeological

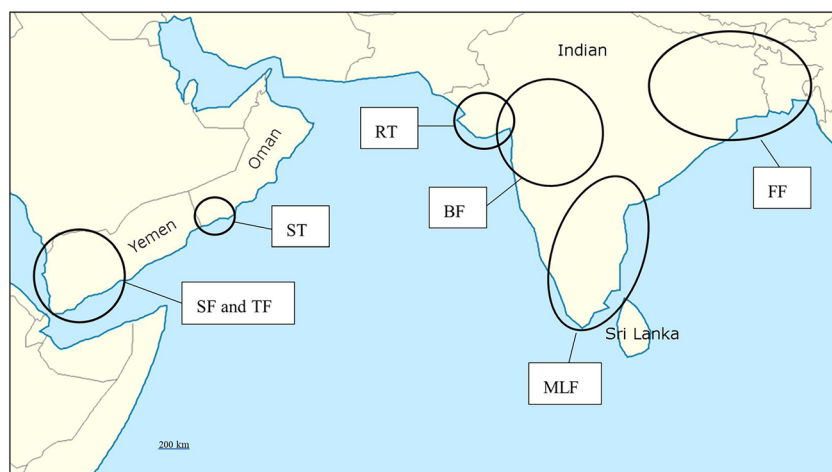


FIGURE 10 Map of the identified area of provenance.

material published by Odelli et al. (2020) and identified as produced in the region of modern-day Tamil Nadu. The Tamil Nadu area, however, is located within a very large igneous and metamorphic formation that includes most of the eastern side of the peninsula (Figure 10). To corroborate the relationship between the MLM group and the southern Indian ceramics, elemental composition comparisons are presented in Figures 11 and 12. The data compared are from published material from the Vellore archaeological site (Naseerutheen et al., 2014) and from archaeological data retrieved from Arikamedu, Chandraketugarh and Tamluck (Das et al., 2017). In both cases, the similarities between the published data and the MLM samples are evident, even if not conclusive. Another characteristic of the MLM group is the great variability noticeable within the group itself. Such limited differences can be interpreted as the result of diversified production centres within a large and geologically similar area or from the variability expected in geological materials. Therefore, to define provenance for the samples, it is imperative to have both further and much more in-depth investigation of the south Indian ceramic products and a larger sample group representative of MLM to map the different production centres and the specific characteristics of the possible different production areas.

On the one hand, stylistic and compositional features refer the SSF group to the Indian Peninsula, but its ambiguous behaviour in the plots (Figures 4 and 5) and the presence of shells result in making the provenance identification uncertain but consistently anchored in coastal areas. Differently from the ST group, the shell fragments in the SSF group are very rounded and well sorted, which could indicate their natural inclusions as material from a coastal environment. Moreover, the sporadic presence of rounded limestone, quartz and feldspars agrees with a coastal sediment source area. The limited concentration of shell fragments and their size being similar to that of other inclusions exclude the possibility of the shells having been added intentionally. Therefore, due to the very common coastal clay nature of the raw material used to produce SSF and the lack of comparable materials and data, it is not possible to define the provenance of the SSF group from an archaeometric point of view without further data collection. Moreover, the analyses here presented and discussed, being a preliminary approach to the topic of the trade network in the Indian Ocean, were limited to the comparison of materials from southern Arabia and the Indian subcontinent. However, other areas of the Indian Ocean region were included in the trade, and the generic nature of the SSF group prevents the authors of this article from excluding any region different from the previously discussed ones.

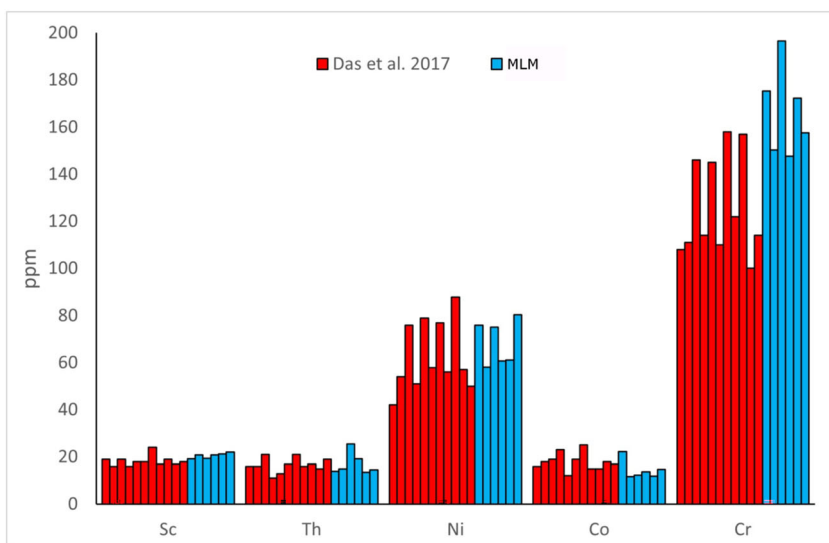


FIGURE 11 Graphic comparison of the samples from MLM (blue) with sample oxide composition from Vellore (yellow) (Naseerutheen et al., 2014).

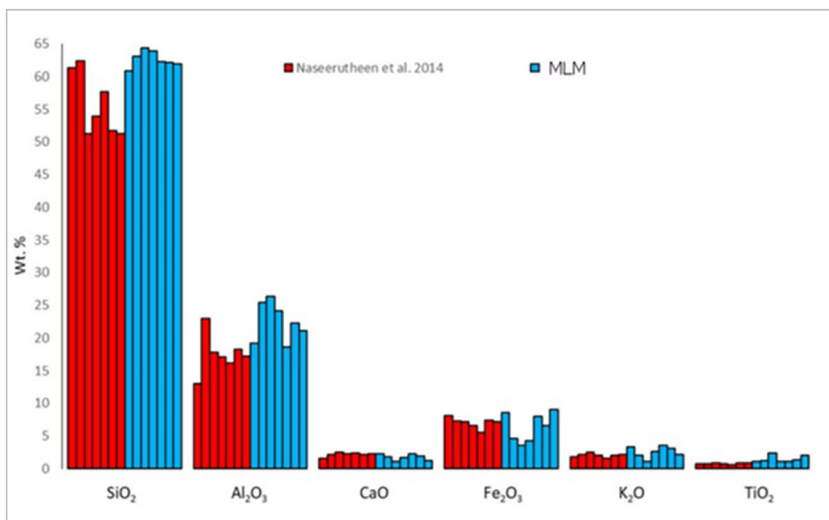


FIGURE 12 Graphic comparison of the samples from MLM (blue) with sample trace element composition from Arikamedu, Chandraketugarh and Tamluk (yellow) (Das et al., 2017).

The multi-analytical approach proposed here, despite its importance in the provenancing study of the material, is also a fundamental source of data for other types of research. For example, PXRD and optical microscopic data can be used to study not only the mineralogical composition of the ceramics but also the technologies adopted for ceramic production and, more precisely, for the firing process. In fact, PXRD allowed for the recognition of mineralogical phases that were not recognizable through optical microscopy, phases that are generally

indicative of the firing temperatures reached in the production of the pottery. In the specific case of this paper, however, despite some characteristics already presented in the 'Results' section, the fabric groups show no evidence of consistent group-related characteristic composition connectable to specific firing temperatures. Nevertheless, the absence of porosity on shell fragments visible in optical microscopy (Karunadasa et al., 2019; Maritan et al., 2007) can be indicative of a firing temperature lower than roughly 750–850°C for the ST, SF and SSF groups.

CONCLUSIONS

The multi-analytical approach applied in this research has demonstrated to be determinant for the material characterization of the ceramics and insightful in the identification of the provenance of most of the samples. The adopted methodology has highlighted a complex classification of the archaeological material, which is complementary to that proposed by Pavan (2017) and Lischi et al. (2022). It results in a distinction between southern Arabia and Indian ceramics comparable to that proposed by those two publications, but it also provides new insights into the production of the pottery and, as a consequence, into the discussion of the material provenance.

The remarkable variability of fabrics found within the site is reflected in the results obtained from several techniques and confirms the very dynamic nature of the trade system that involved Sumhuram and HAS1. Within the 35 samples studied, eight different fabric groups were identified. Integrating all data and comparing with the available published data and major geological regional features allow for tentatively refining the provenance of the samples.

Three groups were identified as originating from the southern Arabian peninsula: ST as possibly local material, SF and TF as from southwestern Arabia. Two groups (BF and RT) have their origin in northwest India, as indicated by the presence of basalts and rice husks, characteristic of ceramics from Gujarat and neighbouring regions. The participation of regions in the southern and northeastern Indian subcontinent in the Indian Ocean trade routes is underlined by the presence of the FF and MLM ceramics. Lastly, for the SSF group, no clear provenance could be established. This research clearly underlines the need to expand the knowledge regarding the ceramic fabrics involved in this trade. This is imperative to be able to increase our understanding of the transported materials and to narrow down the provenance areas even more to create a clearer map of production and distribution of the traded goods.

The importance of adopting a multi-analytical method is evidenced by the preliminary work of fabric provenancing presented in this article and the results proposed by the discussion. The data resulting from the analytical methods adopted prove to be extremely insightful in the characterization of the different fabrics and in their comparison with previously published materials. Caution is required, however, considering the number of samples analysed and the immense geographical area considered, as well as due to the geological complexity and variability. Nevertheless, this paper highlights the potential implications of a multi-analytical methodology not only in providing data but also in proposing new questions regarding the complex cultural and economic exchange in which the settlements of HAS1 and Sumhuram were involved between the third century BCE and the fifth century CE.

ACKNOWLEDGEMENTS

A major thank you goes to the Ministry of Heritage and Tourism of Oman and the Museum of Frankincense Land of Salalah, which, through the DHOMIAP Project, allowed us to study the ceramics from the Khor Rori archaeological site, including both Sumhuram and HAS1. We thank the Italian Ministry of Foreign Affairs and International Cooperation for supporting the

archaeological activity of the DHOMIAP Project. The first author wants to thank the Erasmus + programme, in particular the Erasmus Mundus programme and, more precisely, the master's programme ARCHMAT (Erasmus Mundus Joint Master in Archaeological Material Studies) for the support and the funding provided for the analysis conducted within the context of the final thesis for this master's programme. As members of the ARCHMAT programme, the authors also thank the Sapienza University of Rome and the Aristotle University of Thessaloniki. Special thanks go to the HERCULES Laboratory (10.54499/UIDP/04449/2020 and 10.54499/UIDB/o4449/2020) at the University of Évora and to all its staff for their support and help in the analysis of the samples and the data. Furthermore, the authors seize the opportunity to thank the members of the 'Archaeologists Connected' initiative from Leiden University for their support and Fedor van Rijn for the English editing and proofing. Lastly, the authors are thankful to the anonymous reviewers who provided substantial help in the improvement of the article. Open Access funding enabled and organized by Projekt DEAL.

ORCID

Daniele Zampierin  <https://orcid.org/0000-0003-1646-5438>

Pedro Barrulas  <https://orcid.org/0000-0003-4075-3667>

ENDNOTES

ⁱ Hamr al-Sharqiya 2 (HAS2), not included in the focus of this paper, is also located on the Inqitat plateau, but it does not overlap with HAS1 and is of Islamic foundation and occupation.

ⁱⁱ 'Southwestern Arabia' is the geographic area that nowadays includes Yemen, the Dhofar region of Oman and the southwestern area of Saudi Arabia. The use of 'southwestern Arabia' as a definition aims to delimit the geographical area without including any cultural or political identification.

ⁱⁱⁱ 'India' here refers to the geographical area included within the Indian Subcontinent and what is nowadays Sri Lanka. The use of 'India' as a definition aims to delimit the geographical area without including any cultural or political identification.

^{iv} AFMS.

^v IMTO.

^{vi} DHOFARMap and Inqitat Archaeological Project (<https://dhomiap.cfs.unipi.it/>).

^{vii} All the sample preparation and analysis took place at the HERCULES Laboratory, University of Évora, in Évora (Portugal), except for the thin sections, which were prepared separately at the Geosciences Department of the University of Évora.

^{viii} The 'TS method' developed by Struers consists of the impregnation of the samples using a mixture of EpoResine (in this specific case mixed with EpoDye to highlight the pores) and EpoFix. The proportions used were 500 mL EpoResine (mixed with 2.5 g EpoDye) and 60 mL EpoFix. The samples are left to rest, allowing the resin to penetrate deep into the sample and subsequently solidify. The desired side of the sample is then glued to the glass support, after grinding off the resin covering it. To glue the samples to the glass, resin (coloured with 0.05 g EpoDye) is used. The last step needed, after cutting off a thin section of the sample with a GTS1 Thin Section Cut-Off and Trim Saw, is the grinding and polishing of the samples, to reach 0.03 mm thickness. The larger part of the work is done mechanically with a Logitech PM5 using a mixture of 157.5 g fine silicon powder grit size 600 in 1.5 L water as a grinding agent. When the samples are close to the optimal thickness, a short polishing process is done by hand on a sandpaper grit size 1000 to reach the desired thickness with a nicely polished surface.

^{ix} International Centre for Diffraction Data.

^x The PCA was conducted with all the elements included in Table 6 and in different combinations, but the best result, and hence the best visual representation, was obtained from combining Al_2O_3 , SiO_2 and $CaO + MgO$ values.

^{xi} Rare earth elements.

REFERENCES

- Adams, E. A., Mackenzie, W. S., & Guilford, C. (1984). *Atlas of sedimentary rock under the microscopes*. Longman Group.
- Albright, F. P. (1982). *The American archaeological expedition in Dhofar, Oman, 1952-1953* (Vol. 6). American Foundation for the Study of Man.

- Avanzini, A., & Pavan, A. (2011). Sumhuram, a south Arabian port. In A. Avanzini (Ed.), *Along the aroma and spice routes: The harbour of Sumhuram, its territory and the trade between the Mediterranean, Arabia and India* (pp. 43–56). Bandecchi e Vivaldi.
- Beltrame, M., Liberato, M., Mirão, J., Santos, H., Barrulas, P., Branco, F., Gonçalves, L., Candeias, A., & Schiavon, N. (2019). Islamic and post Islamic ceramics from the town of Santarém (Portugal): The continuity of ceramic technology in a transforming society. *Journal of Archaeological Science: Reports*, 23, 910–928. <https://doi.org/10.1016/j.jasrep.2018.11.029>
- Borowski, M. P., Furmanek, M., Czarniaka, K., & Guida, P. (2015). Steatite-tempered pottery of the stroke ornamented ware culture from Silesia (SW Poland): A neolithic innovation in ceramic technology. *Journal of Archaeological Science*, 57, 207–222.
- Buffa, V. (2019). *Sumhuram: The becoming of the town: Khor Rori report 4*. L'Erma di Bretschneider.
- Das, S. K., Ghosh, S., Gangopadhyay, K., Ghosh, S., & Hazra, M. (2017). Provenance study of ancient potteries from West Bengal and Tamil Nadu: Application of major element oxides and trace element geochemistry. *The Science of the Total Environment*, XLII(2), 11–20.
- Finlay, A. J., McComish, J. M., Ottley, C. J., Bates, C. R., & Selby, D. (2012). Trace element fingerprinting of ceramic building material from Carpow and York Roman fortresses manufactured by the VI legion. *Journal of Archaeological Science*, 39, 2385–2391. <https://doi.org/10.1016/j.jas.2012.03.002>
- Froh, J. (2004). Archaeological ceramics studies by scanning electron microscopy. *Hyperfine Interactions*, 154, 159–176.
- Heimann, R. B., & Maggetti, M. (2019). The struggle between thermodynamics and kinetics: Phase evolution of ancient and historical ceramics. *EMU Notes in Mineralogy*, 20(6), 233–281. <https://www.researchgate.net/publication/337905856>
- Karasik, A., & Smilansky, U. (2008). 3D scanning technology as a standard archaeological tool for pottery analysis: Practice and theory. *Journal of Archaeological Science*, 35, 1148–1168. <https://doi.org/10.1016/j.jas.2007.08.008>
- Karunadasa, K. S. P., Manoratne, C. H., Pitawala, H. M. T. G. A., & Rajapakse, R. M. G. (2019). Thermal decomposition of calcium carbonate (calcite polymorph) as examined by in-situ high-temperature X-ray powder diffraction. *Journal of Physics and Chemistry of Solids*, 134, 21–28.
- Khalifa, M. I. (1988). Geological map of Salalah. Ministry of Petroleum and Minerals, Directorate General of Minerals: Sultanate of Oman.
- Lischi, S. (2018). Inqitat archaeological mission Inqitat archaeological mission fourth and fifth season of the Italian Mission to Oman (IMTO) in season of the Italian Mission to Oman (IMTO) in the site of Inqitat - Khor Rori archaeological site, Dhofar, Sultanate of Oman 28. Unpublished.
- Lischi, S. (2019). Inqitat archaeological mission Inqitat archaeological mission sixth and seven seasons of the archaeological Mission archaeological Mission in the site of Inqitat - Khor Rori archaeological site, Dhofar, sultanate of Khor Rori archaeological site, Dhofar. Unpublished.
- Lischi, S. (2021). Notes on the south Arabian occupation of Inqitat. In G. Hatke & R. Ruzicka (Eds.), *South Arabian long. Distance trade in antiquity: "Out of Arabia"* (pp. 228–244). Cambridge Scholars Publishing.
- Lischi, S. (2022). Settlement dynamics and territorial organization in Dhofar between the bronze age and late antiquity: Understanding the settlement process of the Khor Rori area and development of a new regional cultural model. Unpublished PhD Thesis, University of Pisa.
- Lischi, S. (2023). A first definition of the Dhofar coastal culture. *Ancient Civilizations and Cultural Resources*, 1, 23–38.
- Lischi, S., Odelli, E., Perumal, J. L., Lucejko, J., Ribechini, E., Lippi, M. M., Selvaraj, T., Colombini, M. P., & Raneri, S. (2020). Indian Ocean trade connections: Characterization and commercial routes of torpedo jars. *Heritage Science*, 8, 76. <https://doi.org/10.1186/s40494-020-00425-9>
- Lischi, S., Pavan, A., & Fusaro, A. (2020). Preliminary investigations on the local Pottery in Dhofar (southern Oman) from the Iron age to the Islamic period. *IASA News & Research By Country*, 25, 15–17.
- Lischi, S., Pavan, A., & Fusaro, A. (2022). La ceramica locale in Dhofar (Oman meridionale): Tipi, tecniche produttive e circolazione dall'Età del Ferro al periodo Islamico. *Egitto e Vicino Oriente*, 96, 169–178. <https://doi.org/10.6093/978-88-6719-217-5>
- Magee, P., Barber, D., Sobur, M., & Jasim, S. (2005). Sourcing iron age softstone artefacts in southeastern Arabia: Results from a programme of analysis using inductively coupled plasma-mass spectrometry/optical emission spectrometry (ICPMS/OES). *Arabian Archaeology and Epigraphy*, 16, 129–143.
- Maritan, L. (2019). Archaeo-ceramic 2.0: Investigating ancient ceramics using modern technological approaches. *Archaeological and Anthropological Sciences*, 11, 5085–5093. <https://doi.org/10.1007/s12520-019-00927-z>
- Maritan, L., Angelini, I., Artioli, G., Mazzoli, C., & Saracino, M. (2009). Secondary phosphate in the ceramic materials from Frattesina (Rovigo, North-Eastern Italy). *Journal of Cultural Heritage*, 10, 144–151.
- Maritan, L., Mazzoli, C., & Freestone, I. (2007). Modeling changes in mollusk shell internal micro-structure during firing: Implication for temperature estimate in shell-bearing pottery. *Archaeometry*, 49, 529–541.
- Miriello, D., Bloise, A., De Luca, R., Apollaro, C., Crisci, G. M., Medaglia, S., & Taliano Grasso, A. (2015). First compositional evidences on the local production of Dressel 2–4 amphorae in Calabria (southern Italy): Characterisation and mixing simulations. *Applied Physics A: Materials Science and Processing*, 119, 1595–1608. <https://doi.org/10.1007/s00339-015-9143-y>

- Mirulla, F. (2011). *LA FOTOGRAFIA ARCHEOLOGICA DIGITALE - Dallo Scatto All'elaborazione*. Edipuglia srl.
- Naseerutheen, A., Chandrasekaran, A., Rajalakshmi, A., & Ravisankar, R. (2014). Elemental analysis of ancient potteries of Vellore Dist, Tamil Nadu, India by ED-XRF technique with statistical approach. *Beni-Suef University Journal of Basic and Applied Sciences*, 3, 45–51. <https://doi.org/10.1016/j.bjbas.2014.02.006>
- Odelli, E., Selvaraj, T., Perumal, J., Palleschi, V., Legnaioli, S., & Raneri, S. (2020). Pottery production and trades in Tamil Nadu region: New insights from Alagankulam and Keeladi excavation sites. *Heritage Science*, 8, 1–13. <https://doi.org/10.1186/s40494-020-00402-2>
- Pallecchi, P., & Pavan, A. (2011). Local raw materials used by craftsmen and in the development of the city of Sumhuram. In A. Avanzini (Ed.), *Along the aroma and spice routes: The harbour of Sumhuram, its territory and the trade between the Mediterranean, Arabia and India* (pp. 81–95). Bandecchi e Vivaldi.
- Pandey, R. K., Pandey, R. J., & Akram, M. (Eds.). (2017). *Geography of India*. Uttarakhand Open University.
- Pavan, A. (2017). *A cosmopolitan city on the Arabian coast: The imported and local pottery from Khor Rori: Khor Rori report 3*. L'Erma di Bretschneider.
- Powers, R. W., Ramirez, L. F., Redmond, C. D., & Elberg, E. L. Jr. (1966). Geology of the Arabian peninsula sedimentary geology of Saudi Arabia. US Geological Survey Professional Paper 560-D: 154.
- Quinn, P. S., Burton, M. M., Broughton, D., & van Heymbeek, S. (2013). Deciphering compositional patterning in plainware ceramics from late prehistoric hunter-gatherer sites in the peninsular ranges, San Diego County, California. *American Antiquity and Latin American Antiquity* 289-07-305.
- Reddy, A. (2015). Sourcing Indian ceramics in Arabia: Actual imports and local imitations. *Proceedings of the Seminar for Arabian Studies*, 45, 253–272.
- Seetha, D., & Velraj, G. (2016). Characterisation and chemometric analysis of ancient pot shards trenched from Arpakkam, Tamil Nadu, India. *Journal of Applied Research and Technology*, 14, 345–353. <https://doi.org/10.1016/j.jart.2016.08.002>
- Sun, S. S., & McDonough, W. F. (1989). Chemical and isotopic systematics of oceanic basalts: Implications for mantle composition and processes. *Geological Society, Special Publication*, 42, 313–345.
- Tite, M. S. (1991). The impact of electron microscopy on ceramic studies. *Proceedings of the British Academy*, 77, 111–131. <https://www.thebritishacademy.ac.uk/sites/default/files/77p111.pdf>
- Tite, M. S., Freestone, I. C., Meeks, N. D., & Bimson, M. (1982). The use of scanning electron microscopy in the technological examination of ancient ceramic. In J. Olin & A. Franklin (Eds.), *Archaeological ceramics* (p. 256). Smithsonian Institution Press.
- Tomber, R., Cartwright, C., & Gupta, S. (2011). Rice temper: Technological solutions and source identification in the Indian Ocean. *Journal of Archaeological Science*, 38, 360–366.
- Tsoupra, A., Clist, B., da Conceição Lopes, M., Moita, P., Barrulas, P., da Piedade de Jesus, M., da Silva Domingos, S., Bostoen, K., & Mirão, J. (2022). A multi-analytical characterization of fourteenth to eighteenth century pottery from the Kongo kingdom, Central Africa. *Scientific Reports*, 12, 9943. <https://www.nature.com/articles/s41598-022-14089-x>
- Wadia, D. N. (1919). *Geology of India*. Macmillan and Co.
- Zarins, J. (2001). *The land of incense: Archaeological work in the governorate of Dhofar, Sultanate of Oman, 1990–1995: The project of the National Committee for the supervision of archaeological survey in the sultanate Ministry of Information*. Sultan Qaboos University Publications.
- Zerboni, A., Perego, A., Mariani, G. S., Brandolini, F., Al Kindi, M., Regattieri, E., Zanchetta, G., Bergi, F., Charpentier, V., & Cremaschi, M. (2020). Geomorphology of the Jebel Qara and coastal plain of Salalah (Dhofar, southern Sultanate of Oman). *Journal of Maps*, 16(2), 187–198.

How to cite this article: Zampierin, D., Moita, P., Lischi, S., van Aerde, M., Barrulas, P., & Mirão, J. (2024). A multi-analytical approach applied to pottery from Oman as a key to understanding ancient Indian Ocean maritime trade. *Archaeometry*, 66(5), 967–1015. <https://doi.org/10.1111/arcm.12949>